Naval Surface Warfare Center

Carderock Division

West Bethesda, MD 20817-5700

NSWCCD-80-TR-2019/036 **November 2019**

Naval Architecture and Engineering Department

Technical Report

R/V ATHENA MODEL (5365) IN CALM WATER

by

Anne Fullerton, Jayson Geiser, Sarah Punzi, Jason Morin, Charles Weil, Don Walker, Evan Lee, and Craig Merrill

NSWCCD

DISTRIBUTION STATEMENT A: Approved for public release; distribution unlimited.

NSWCCD-80-TR-2919/036 *R/V Athena* Model (5365) in Calm Water

REPORT DOCUMENTATION PAGE

Form Approved
OMB No. 0704-0188

1. REPORT DATE *(DD-MM-YYYY)*
16-11-2019

2. REPORT TYPE
Final

3. DATES COVERED *(From - To)*
Apr 2015-Oct 2016

4. TITLE AND SUBTITLE
R/V Athena Model (5365) in Calm Water

5a. CONTRACT NUMBER
N0001416WX00664

5b. GRANT NUMBER

5c. PROGRAM ELEMENT NUMBER

6. AUTHOR(S)
Anne Fullerton, Jayson Geiser, Sarah Punzi, Jason Morin, Charles Weil, Don Walker, Evan Lee, and Craig Merrill

5d. PROJECT NUMBER

5e. TASK NUMBER

5f. WORK UNIT NUMBER
100001147500

7. PERFORMING ORGANIZATION NAME(S) AND ADDRESS(ES)

Naval Surface Warfare Center
Carderock Division (Code 833)
9500 Macarthur Boulevard
West Bethesda, MD 20817-5700

8. PERFORMING ORGANIZATION REPORT NUMBER

NSWCCD-80-TR-2019/036

9. SPONSORING / MONITORING AGENCY NAME(S) AND ADDRESS(ES)
Dr. Robert Brizzolara, ONR 333
Office of Naval Research
875 North Randolph Street
Arlington, VA 22203-1995

10. SPONSOR/MONITOR'S ACRONYM(S)

11. SPONSOR/MONITOR'S REPORT NUMBER(S)

12. DISTRIBUTION / AVAILABILITY STATEMENT
DISTRIBUTION STATEMENT A. Approved for public release; distribution unlimited.

13. SUPPLEMENTARY NOTES

14. ABSTRACT
Current structural design methods for high speed naval craft rely heavily on empiricism. To support this understanding, a computational approach to predicting motions and loads was proposed. As part of this study, Model 5365 was tested in calm water, regular waves, and irregular waves. This report focuses on the analysis of the calm water data, and the accompanying uncertainty analysis.

15. SUBJECT TERMS
R/V Athena, model 5365, resistance, heave, sinkage, trim, semi-planing, uncertainty analysis, CFD validation data set

16. SECURITY CLASSIFICATION OF:			17. LIMITATION OF ABSTRACT	18. NUMBER OF PAGES	19a. NAME OF RESPONSIBLE PERSON
					Alma Jacobson
a. REPORT	**b. ABSTRACT**	**c. THIS PAGE**			**19b. TELEPHONE NUMBER** *(include area code)*
Unclassified	Unclassified	Unclassified	See 12.	viii+54	757-492-4235

Standard Form 298 (Rev. 8-98)
Prescribed by ANSI Std. Z39.18

THIS PAGE INTENTIONALLY LEFT BLANK

CONTENTS

CONTENTS iii
SYMBOLS, ABBREVIATIONS, AND ACRONYMS v
ADMINISTRATIVE INFORMATION viii
ACKNOWLEDGEMENTS viii
SUMMARY 9
INTRODUCTION 10
EXPERIMENTAL APPROACH 11
  Facility Description 11
  Model Description 11
  Test Conditions 16
EXPERIMENTAL METHODS 17
  Visualization 17
  Forces and Moments 17
  Motions 17
  Sinkage and Trim 19
  Carriage Speed 19
  Data Collection 19
  Test Procedures 20
RESULTS AND DISCUSSION 21
  Uncertainty Analysis Estimates 21
  Mass Properties 21
  Resistance 22
  Sinkage and Trim 22
  Dynamic Wetted Hull Surface Area 25
CONCLUSIONS 32
RECOMMENDATIONS 32
REFERENCES 33
APPENDIX A: DYNAMOMETER CALIBRATIONS A-1

APPENDIX B: SWINGING PROCEDURE....B-1

APPENDIX C: *ATHENA* CALM WATER MODEL TEST – UNCERTAINTY ANALYSIS C-1

FIGURES

Figure 1. Full Scale *R/V Athena*....12

Figure 2. Laser Tracker Surface Measurements of Model 5635 (Largest Deviation is 0.04 Inches as Shown in Red)....13

Figure 3. Photograph of Model 5365 Showing the Yellow and Black Paint Scheme, Waterlines, and Station Lines 13

Figure 4. As-Installed IMU....18

Figure 5. Screenshot of the LabVIEW Data Acquisition Program....20

Figure 6. Sketch of *Athena* Model with String Potentiometers in Initial Condition (Not to Scale, Hull Geometry is Notional) 23

Figure 7. Sketch of Trimmed *Athena* Model with String Potentiometers (Not to Scale, Hull Geometry is Notional) 24

Figure 8. Running Waterline at 6.3 knots (Fr=0.43) 26

Figure 9. Running Waterline and Bow Spray Sheet at 14.5 knots (Fr=1.00)....26

Figure 10. Trim Comparison of String Potentiometer Calculations and IMU (Kearfott) Measurements....31

TABLES

Table 1. *Athena* Model As-Tested Characteristics (July 2015) 14

Table 2. *Athena* Model Hull Form Data Determined from Hydrostatic Analysis....15

Table 3. *Athena* Model Test Conditions....16

Table 4. Uncertainty in As-Tested Mass Properties 21

Table 5. Values for String Potentiometer Positions....24

Table 6. Uncertainty and Values for Resistance Calculations....27

Table 7. Uncertainty and Values for Total Resistance Coefficient Calculations 27

Table 8. Uncertainty and Values for Friction Resistance Coefficient Calculations 28

Table 9. Uncertainty and Values for Residuary Resistance Coefficient Calculations....28

Table 10. Uncertainty and Values for Trim Calculations....29

Table 11. Uncertainty and Values for Sinkage at Tow Point Calculations 29

Table 12. Uncertainty and Values for Carriage Speed 30

SYMBOLS, ABBREVIATIONS, AND ACRONYMS

3-DOF ... Three degrees-of-freedom
6-DOF ... Six degree-of-freedom
+ABL ... Positive values above the baseline
AP ... Aft perpendicular
ASP ... Aft string potentiometer
B ... Beam or Bias uncertainty
BWL ... Beam along the waterline
C_B ... Block coefficient
C_F ... Friction resistance coefficient
CFD ... Computational Fluid Dynamics
CL ... Centerline
CP ... Prismatic coefficient
C_R ... Residuary resistance coefficient
C_T ... Total resistance coefficient
D ... Depth or Reported Mean Value
DAS ... Data Acquisition System
E ... Error
+FAP ... Positive values forward of the aft perpendicular
Fr ... Length Froude Number, $Fr = \frac{U}{\sqrt{gLWL}}$
fps ... Feet per Second
f_s ... Data sampling rate
FSP ... Forward sting potentiometer
ft ... foot/feet
fwd ... Forward
F_x ... Longitudinal resistance from a dynamometer
F_z ... Vertical resistance from a dynamometer
g ... Gravitational acceleration, g=32.174 ft/s^2
GPS ... Global Positioning System

H_s, $H_{1/3}$, H_{m0} .... Significant wave height
Hz .... Hertz or cycle per second
in .... inch(es)
IMU .... Inertial Measurement Unit
I_y .... Pitch moment of inertia
k_y .... Pitch gyradius
lb, lbs, or lbf .... pound(s) force
LCB .... Longitudinal Center of Buoyancy
LCG .... Longitudinal Center of Gravity
LTP .... Longitudinal center of Tow Point
LBP or L_{PP} .... Length between perpendiculars
LWL .... Length of the waterline
NI .... National Instruments Corporation
NSWCCD .... Naval Surface Warfare Center Carderock Division
ONR .... Office of Naval Research
P .... Precision uncertainty
+PCL .... Positive values port from the centerline
r^2 .... Pearson's correlation coefficient
R_t .... Total resistance
s .... Sample standard deviation
S_o .... Static wetted surface area
T .... Draft or target value
T_{CG} .... Draft at center of gravity
T_m, T_p, ... Modal, or peak, wave period
U .... Total uncertainty or model speed
V .... Volume or model speed
VCG .... Vertical Center of Gravity
VTP .... Vertical center of Tow Point
Δ .... Displaced weight
θ .... Static trim angle or sensitivity coefficient
ν .... Kinematic viscosity
σ .... Heave or sinkage, or population standard deviation
τ .... Running trim angle

ν .... Degrees of freedom

∇ .... Displace volume

ADMINISTRATIVE INFORMATION

The work described in this report was performed by the Naval Architecture and Engineering Department (Code 80) at the Naval Surface Warfare Center, Carderock Division (NSWCCD). The work was funded by the Office of Naval Research (ONR), Code 333, (N0001416WX00664) under the direction of Dr. Robert Brizzolara.

ACKNOWLEDGEMENTS

The authors would like to thank Dan Hayden, David Bochinski, and Lawrence Snyder for their valuable assistance during model preparation and testing, as well as Dr. Thomas Fu for his valuable guidance during planning and testing.

SUMMARY

Current structural design methods for high speed naval craft rely heavily on empiricism. Though these methods have been employed reliably for a number of years, it is likely that an unknown level of conservatism exists in the prediction of both global and local impact loads to ensure the vessel's structural design is robust. A better physical understanding of the dynamic response of high speed craft in seas would allow for increased structural optimization. To support this understanding, a computational approach to predicting motions and loads was proposed. The publicly releasable hull form Naval Surface Warfare Center Carderock Division (NSWCCD) Model 5365 (*R/V Athena*) was chosen to facilitate release of results to various computational teams. As part of this study, Model 5365 was tested in calm water, regular waves, and irregular waves in 2014. After reviewing data from that test, it was determined that the Athena model (NSWCCD Model 5365) should be modified to enable towing from the longitudinal center of gravity and allow increased sea state conditions to be tested. Model 5365 was then modified and re-tested in calm water with added speed range, regular waves, and irregular waves. This report focuses on the analysis of the calm water data, and the accompanying uncertainty analysis. Comparisons of the 2015 data with simulations and historical test data of Model 5365 is not within the scope of this report.

Uncertainty estimates for resistance and trim are small, while uncertainty measurements for sinkage are larger. The applied lessons learned from the 2014 test [1] (longer basin settling times) appeared to reduce the precision uncertainty in this 2015 test. Even longer test runs and longer settling times may help further reduce sinkage uncertainty for future testing, if necessary. The unbalanced bias (*B*) and precision (*P*) uncertainties for trim (i.e. $P\tau >> B\tau$) are considered acceptable since the total trim uncertainty is small. The translation of the tow point allows for a more accurate representation of full scale motions. At full scale, the craft would pitch about the center of gravity and moving the tow point to the center of gravity allows the model to pitch about the center of gravity. Moving the tow point also eliminates the uncertainty of the complex motion of the model in CFD simulations when towed from the 2014 tow point.

The methods for determining the location of the running waterline and determination of the dynamic wetted surface area could be improved if frictional and residuary components of resistance at full scale are an important test objective. Underwater photographs that are extracted from video need a significant amount of lighting (intensity and number of lights). There is a tradeoff between the ease of staging underwater fixtures directly on the basin bottom and the reduced lighting needs when staging is constructed at a lower depth.. This issue could be mitigated if available time and resources were available to better optimize the underwater staging; and using lower power, high intensity, LED lights suitable for underwater operation. Additional above water cameras could be strategically placed on the carriage to observe the separation of the bow spray sheet from the hull surface. Several trial runs would be needed to identify the hull location to focus a camera and where a camera could be secured to the underside of the carriage.

INTRODUCTION

The objective of the 2015 *Athena* model test was to improve understanding of the dynamic response of semi-planing craft in a seaway. Specifically, data were collected to:

1. Evaluate the ability of experimental techniques to capture semi-planing vessel response in two degrees-of-freedom (heave and pitch motions, as well as their associated velocities and accelerations).
2. Provide data for comparison with numerical predictions of dynamic response of semi-planing craft in a seaway.
3. Support the future design of a secondary loads *Athena* model, and later a structural model that will be used to collect higher fidelity hydrodynamic loading data.

This test is the second in a series of tests of the *Athena* model hull form for the ONR hydrodynamic research project. The first test was completed in November 2014. After reviewing data from that test, it was determined that the *Athena* model (NSWCCD Model 5365) should be modified to enable towing from the longitudinal center of gravity and allow increased sea state conditions to be tested. Additionally, the data collection rates were increased to capture the unsteady hydrodynamic forces measured by the hull-mounted pressure sensors. This report will focus on the calm water results; subsequent reports will present results from model testing in waves and comparisons of the measurements with predictions. Comparisons of this data with simulations and historical test data of Model 5365 is not within the scope of this report. The calm water results will be used for comparison with numerical predictions as a first step to meet objective two by showing that the numerical predictions can calculate the steady state solutions of a calm water simulation.

EXPERIMENTAL APPROACH

Facility Description

Measurements of the *Athena* model operating in calm water, regular, and irregular waves were performed in the Deep Water Basin at NSWCCD using towing Carriage 2. The basin is approximately 1886 feet long, 50.96 feet wide, and 22 feet deep. Carriage 2 has a maximum towing speed of 20 knots (33.8 feet/second). A pneumatic wavemaker is located at the east end of the basin, with a wave absorbing beach at the west end.

Model Description

Model 5365 is an 8.25 scale model of the *R/V Athena*, shown in Figure 1. The *R/V Athena* is a converted *PG-84 Asheville-Class* patrol gunboat which is operated out of Naval Surface Warfare Center, Panama City Division, as a high speed research vessel. The model, built in 1979, was constructed out of wood and fiberglass. The model has been refurbished over its lifetime, and in 2002 it was measured using NSWCCD's laser tracker model measurement system. The detailed measurements of the model, shown in Figure 2 revealed an asymmetry in the hull in the region of the bow, on the starboard side of the model. This as-measured geometry is available from NSWCCD by request as an IGES geometry file.

The model was refurbished again in 2015 in preparation for this test. As a part of the refurbishment, the tow-point of the model was moved to align with the center of mass. This translation of the tow point allows for a more accurate representation of full scale motions, and more comparable measurements to the CFD simulations. A one inch square checkerboard grid (shown in Figure 3) was added to enable better images of the wetted surface area during testing. Turbulence stimulators were placed on the model along a line two inches aft of and parallel to the leading edge of the bow. The turbulence stimulators are acrylic cylinders, 1/8 inch high, with a diameter of 1/8 inch. Table 1 shows the as-tested model scale particulars. The model was ballasted to a center of gravity to achieve the same waterline used during the 2014 tests [1]. The pitch radius of gyration is estimated to be one quarter of the waterline length (0.25*LWL). This estimation has been used for combatant raft when the actual pitch radius of gyration is unknown. The pitch mass moment of inertia was set to achieve the desired pitch radius of gyration. Table 2 shows the data from the hydrostatic analysis at the ballasted condition.

A discrepancy between the marked waterline and the IGES geometry file was discovered, when verifying hydrostatic equilibrium with the observed sinkage and trim. After leveling the model on a calibration bench and re-scanning the hull, the marked waterline had a trim (pitch) angle discrepancy of 0.16 degrees of trimmed down by the bow. The sinkage and trim values in this report are relative this initial hydrostatic trim condition. The initial hydrostatic condition was determined using the as-tested measurements of model weight and center of gravity. The geometry file used for CFD comparisons and hydrostatic equilibrium are oriented parallel to the baseline defined in the lines plan, shown in Figure 1.

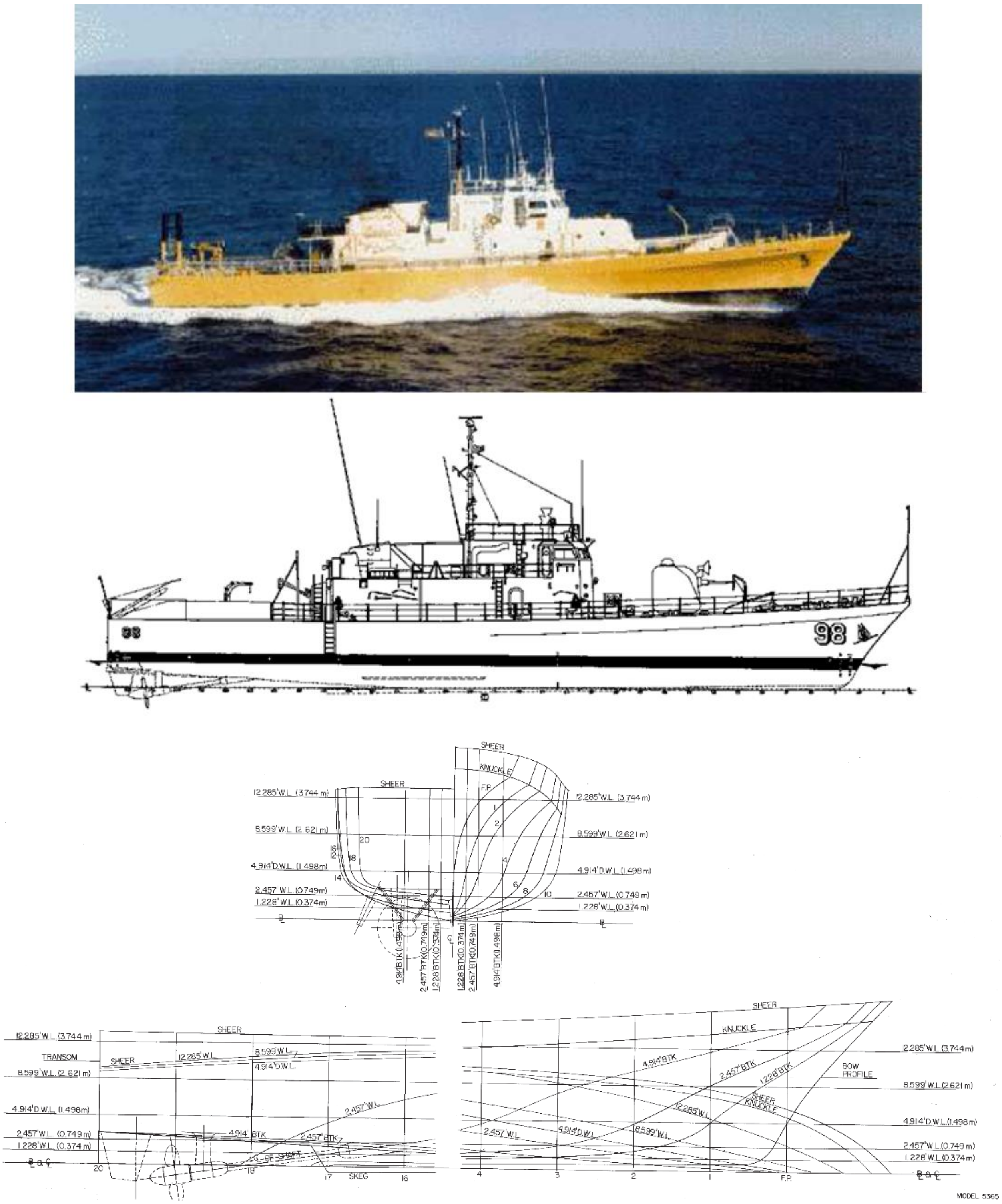

Figure 1. Full Scale *R/V Athena*

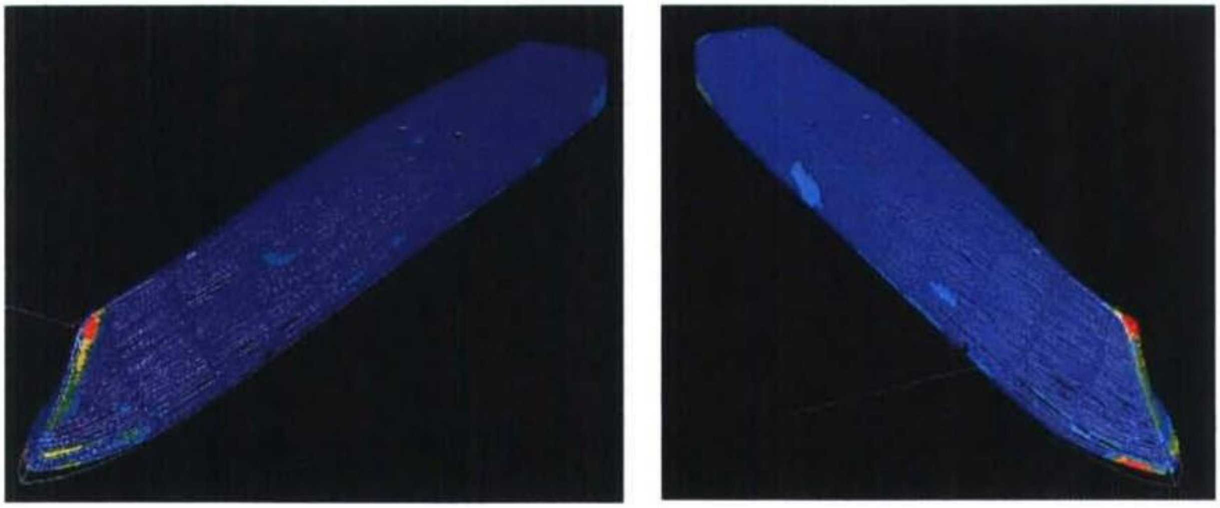

Figure 2. Laser Tracker Surface Measurements of Model 5635 (Largest Deviation is 0.04 Inches as Shown in Red)

Figure 3. Photograph of Model 5365 Showing the Yellow and Black Paint Scheme, Waterlines, and Station Lines

Table 1. *Athena* Model As-Tested Characteristics (July 2015)

Parameter	As-Tested Value (D) ± Uncertainty (U)
Scale Ratio	8.25
Degrees of Freedom	Heave, Trim
Displacement, Δ	858.00 ± 0.30 (lbf)
As-Tested Basin Water Density at 74.01±0.30°F, ρ	1.93415 ± 0.0011 (slugs/ft^3)
As-Tested Basin Kinematic Viscosity at 74.01±0.30°F, ν	10.001 ± 0.066 *10^6(ft^2/s)
Displaced Volume, $\nabla=\Delta/\rho*g$	13.7887 ± 0.0092 (ft^3)
Static Trim Angle from Baseline*, (θ (+bow up)	0.119 ± 0.020°
Longitudinal Center of Gravity, LCG (+FAP)	96.024 ± 0.082 (inch)
Vertical Center of Gravity, VCG (+ABL)	9.74 ± 0.38 (inch)
Longitudinal Center of Tow Point, LTP (+FAP)	97.381 ± 0.063 (inch)
Vertical Center of Tow Point, VTP (+ABL)	10.040 ± 0.063 (inch)
Pitch Mass Moment of Inertia, $I_{y,CG}$ (about CG)	18,536 ± 339 (lbf-ft^2)
Pitch Radius of Gyration, $k_{y,CG}$ (about CG)	55.78 ± 0.51 (inch)
Length Between Perpendiculars, LBP	224.000 ± 0.036 (inch)
Length of the Waterline*, LWL	224.227 ± 0.040 (inch)
Length Overall, LOA	238.308 ± 0.036 (inch)
Beam Overall, BOA	35.044 ± 0.036 (inch)
Depth Overall, D	25.353 ± 0.036 (inch)
Maximum Waterline Beam*, BWL (near STA 14)	33.218 ± 0.040 (inch)
* Indicates that value was determined from hydrostatic analysis and not measured directly +FAP = positive values forward of the aft perpendicular +ABL = positive values above the baseline	

Table 2. *Athena* Model Hull Form Data Determined from Hydrostatic Analysis

Parameter	As-Tested Value
Longitudinal Center of Buoyancy, LCB (+FAP)	95.917 (inch)
Area of the Waterplane, A_{WP}	37.79 (ft^2)
Immersed Area of Midship Section, A_M	157.8 ($inch^2$)
Midship Waterline Beam, B_M	30.12 (inch)
Baseline Draft at Midship, T_M	7.321 (inch)
Hull Draft at Midship, T_M'	7.233 (inch)
Immersed Area of Maximum Section, A_X (at STA 12)	169.2 (in^2)
Waterline Beam at Maximum Section, B_X (at STA 12)	31.12 (inch)
Hull Draft at Maximum Section, T_X	7.160 (inch)
Waterline Beam at Transom, B_T	27.21 (inch)
Hull Draft at Transom Section, T_T	3.302 (inch)
LCB/LWL (+FAP)	0.428
LCG/LWL (+FAP)	0.428
LWL/LBP	1.001
LWL/BWL	6.750
LWL/B_X	7.206
LWL/T_M	30.63
B_X/T_X	4.346
Slenderness Ratio, LWL^3/∇	7.792
Block Coefficient, $C_B=(\nabla/LWL*B_X*T_X)$	0.477
Prismatic Coefficient, $C_P=\nabla/A_x*LWL$	0.628
Midship Sectional Area Coefficient, $C_M=A_M/B_M*T_M$	0.716
Maximum Sectional Area Coefficient, $C_X=A_X/B_X*T_X$	0.759
Vertical Prismatic Coefficient, $C_{VP}=\nabla/T_X*A_{WP}$	0.612
Static Wetted Surface Area, S_o	46.14 (ft^2)
Wetted Surface Coefficient, $C_S=S_o/LWL*(2*T_X+B_X)$	0.6521
Slenderness Ratio, LWL^3/∇	7.792
+FAP = positive values forward of the aft perpendicular +ABL = positive values above the baseline	

Test Conditions

The Athena model was tested in calm water, regular waves, and irregular waves at a variety of speeds. The target test conditions are listed in Table 3. Conditions tested in 2014 are highlighted in yellow. Ambient conditions during the test were nominally a 74°F basin water temperature, 80°F air temperature, and an 80% relative humidity. The calm water speeds were chosen to match resistance, sinkage, and trim curves from previous model tests [1]. Additional calm-water speeds were added to increase the resolution of the predicted resistance, sinkage, and trim curves. Also, a planing speed was added to upper end of the test matrix.

Table 3. *Athena* Model Test Conditions

Speed (kts)	Fr	Wave Type	Wave Height, H_s (inch)	Wave Period, T_p
2.0	0.14	Calm		
3.1	0.22	Calm		
3.7	0.25	Calm		
4.2	0.29	Calm		
6.3	0.43	Calm		
7.7	0.53	Calm		
9.0	0.62	Calm		
12.2	0.84	Calm		
14.5	1.00	Calm		

EXPERIMENTAL METHODS

Visualization

Digital video cameras with a frame rate of 30 fps were used to record the motion of the free surface and flow separation from multiple views. The standard views included a starboard profile view, a starboard stern quartering view, and a bow view. Video was digitized and backed up during testing. Underwater video was collected during calm water test runs to characterize the wetted surface area. The underwater camera location had a limited perspective of the bow spray sheet and the waterline elevation along the mid body. This limited perspective did not permit a quantitative estimate of the wetted surface along the painted checkerboard grid. The above water profile view does show the wetted waterline along the painted checkerboard grid, but the spray sheet does obscure a portion of the wetted waterline and prevents a quantitative evaluation of the wetted surface area.

Forces and Moments

The 6-DOF force and moment measurements were acquired through two separate dynamometers mounted on the model. The main dynamometer was attached to the model above the tow point and measured the forces and moments in an Earth fixed orientation during testing. There was an additional dynamometer mounted at the model's stern and connected to a grasshopper fixture. The grasshopper fixture is a balanced flexible arm which is designed to apply minimal vertical forces and is used to restrict yaw motions of the model. Because this additional fixture can absorb some of the drag forces, the dynamometer measures forces exerted on the fixture to determine the total drag on the model. Since the dynamometer is installed below the grasshopper fixture, the forces exerted on the fixture are measured in the body fixed orientation. These body fixed forces are transformed to an Earth fixed orientation before used to calculate the total drag on the model. The dynamometers were manufactured at NSWCCD using four 3-axis Kistler force sensors (Type 9602A3211). Four sensors are used in each 6-DOF system to increase accuracy, effective range, and durability during testing. These sensors have an effective range of approximately ±500 pounds in the x and y direction, and ±900 pounds in z at 100% full scale, but can be switched to operate at 10% of full scale (±50 pounds in the x and y, and ±90 pounds in z). At full scale, the resolution is 0.45 pounds for x and y, and 0.41 pounds in z. The standard error for both scales is ±5%. Conversion between voltage and force measurements was performed via a matrix calibration to remove crosstalk between the sensors. The calibration was conducted using a custom 6 DOF calibration rig fabricated at NSWCCD. A more detailed description of the dynamometers and calibration is included in APPENDIX A:.

Motions

A Kearfott KN-5050 inertial measurement unit (IMU) was used to measure the 3-DOF angular positions and angular rates. This IMU consists of a ring laser gyro and employs GPS position aiding when GPS signals were available. The position aiding feature was not used for this test effort since GPS position signals were not available indoors. This IMU provided a kinematic state estimate using an onboard Kalman filter algorithm that outputs digital sentences at a data rate of 50 Hz.

The IMU was rigidly mounted to a platform (Figure 4) and provided measurements of the model's pitch, pitch rate, heave, heave rate and longitudinal and vertical acceleration. Angular offsets between the as-installed IMU and the model baseline were measured using a handheld inclinometer (Pro360) and compared with the trim and heel angle results at hydrostatic equilibrium. The as-installed trim offset measured using handheld inclinometer was 0.3 degrees down by the bow. The IMU average trim angle for all the static floating runs 0.389 degrees down by the bow. These two offset measurements were consistent with the offset trend when comparing to the trim angle calculated from the string potentiometers.

The Kearfott inertial measurement unit provided kinematic data as a RS-422 serial stream. The RS-422 protocol was converted to a RS-232 protocol and then passed through a Lantronix UDS 2100 serial to Ethernet converter. The Lantronix UDS 2100 converter was connected to the network switch and collected directly by the data acquisition computer. The IMU bias uncertainty for heading was ±0.84°and the roll/pitch accuracy bias uncertainty was ±0.056° at a 95% confidence level. The IMU outputs data at 50 Hz.

Figure 4. As-Installed IMU

Sinkage and Trim

Two string potentiometers (string pots) were used to measure vertical displacement of the model at the bow and the stern. The string potentiometers used were UniMeasure model PA-50-004, which had a 50-inch range and a maximum error of ±0.125-inch. These potentiometer measurements provided tow post sinkage (heave) and running trim (pitch) angle via trigonometry calculations using the known locations of string connections relative to the tow post gimbal. This calculated tow post sinkage and running trim are reported as the changes from the floating static condition, which does not include the initial tow post position below the waterline nor the hydrostatic trim angle. The string potentiometers were attached using eye screws that were mounted as far apart as possible to increase the accuracy of the trigonometry calculations for tow post sinkage and trim. The aft string potentiometer was mounted on the transom, or 0.0 inches forward of the aft perpendicular. The forward string potentiometer was mounted 237.46 inches forward of the aft perpendicular. The calculated running trim angle from the string potentiometer was found to have a lower total uncertainty than the IMU pitch measurements, and was considered the best value for reporting running trim angle in calm water.

The output voltage from the string potentiometers were converted to inches of displacement with positive values for retracting string displacement (upward heave). The potentiometer analog voltage signals were zeroed prior to each test run while the model was floating statically to control for the uncertainty typically present in this type of sensor (signal drift). Zeroing the analog voltage provided hull vertical displacement measurements relative to the static waterline. These measurements were collected as analog signals at a sampling rate of 6,250 Hz with a 20 Hz oscillation limit for the mechanical tensioner.

Carriage Speed

Carriage 2 is equipped with a wheel encoder that has been calibrated to output carriage speed. This carriage speed signal was collected by the data acquisition system. Carriage speed uncertainty estimates were taken from the calibration documentation available onboard the carriage.

Data Collection

The data acquisition system (DAS) consisted of two National Instruments (NI) 9188 cDAQ chassis configured to collect analog and digital signals. The two NI 9188 cDAQ chassis were hardware synced using NI 9469 modules. The data from the sensors were collected and stored on a standalone computer connected to the cDAQ chassis via an 8 port 1 Gigabyte network switch. Most DAS channels for this test were collected as analog signals that were conditioned and sampled via NI modules (model No. 9239) that simultaneously sample four-channels at 24-bit delta-sigma analog-to-digital conversion (ADC) resolution. These NI 9239 modules employ a combination of analog and digital filtering to reject out-of-band signals and provide for anti-aliasing. NI 9239 modules prevent signal aliasing with a hardware low-pass pre-filter along with an on-module digital filter that was automatically configured based on the digital sampling rate. Analog signals were collected at a sampling rate (f_s) of 6,250 Hz giving an effective acquired signal bandwidth of approximately 0 to 3,125 Hz. This signal bandwidth may be further reduced depending on the response characteristics of a particular sensor.

A data acquisition program (titled DAQ 5.0) developed at NSWCCD using LabVIEW 2014 was used to control the data acquisition chassis, modules, signal zeroing, signal conversion to engineering values, and the data collection. An example display of this program interface is shown in Figure 5. All the analog and digital channels were hardware synced in time using the master time base clock on the cDAQ chassis. The data acquisition program collected two sets of data. A raw voltage data set was collected during the entire run (PASS file). Simultaneously, an engineering value data set (with zeroing and calibration factors applied) was calculated during steady state sections of the run which were selected by the operator (SPOT file).

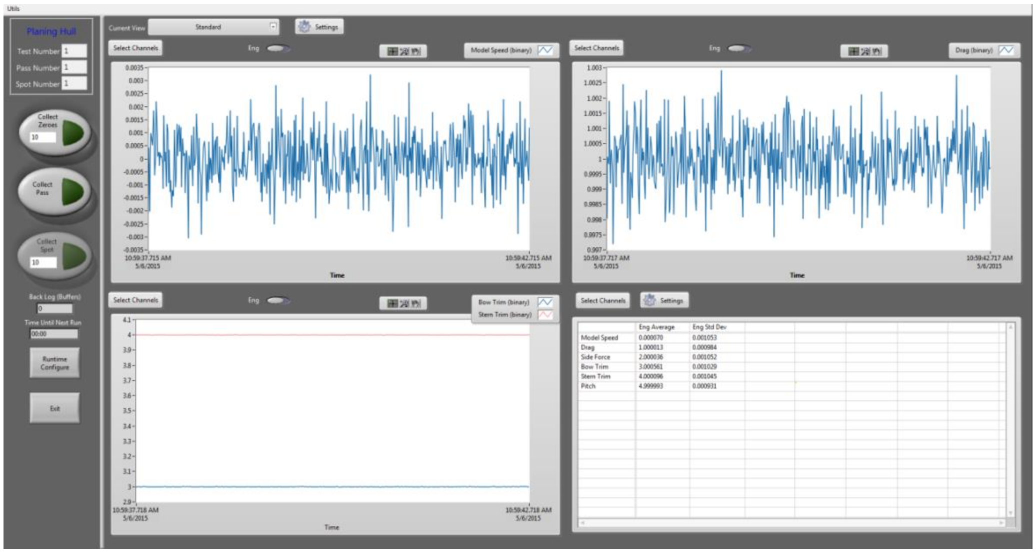

Figure 5. Screenshot of the LabVIEW Data Acquisition Program

Test Procedures

The calm water runs began with the model in a floating, zero speed condition. A ZERO data file was collected in this floating static condition before the moving the carriage. Then the test engineer started a PASS file data collection, followed by the carriage operator manually accelerating the carriage to the target steady speed. The carriage operator signaled the test engineer when the target steady speed was achieved. The test engineer then initiated a SPOT file data collection for a pre-configured collection duration of 10 seconds. To minimize the duration of the test, two SPOT files were collected during one pass of the carriage along the basin. The target speeds for each of the SPOT files were selected in an irregular pattern from the test matrix to promote independent sampling. The second SPOT file collected during a pass was always at a faster speed than the first SPOT file target speed. This was done so that the second, faster, target speed involve accelerating the carriage away form the wake associated with the first, slower, target speed. As the carriage approached the basin safety stops, the operator signaled to the test engineer before manually decelerating the carriage to a stop at the end of the basin. The basin waves had an approximate settling time of 30 minutes between runs with the longitudinal wave dampers deployed. The 2014 test [1] showed that longer settling time reduced the standard deviation of the results within each run.

RESULTS AND DISCUSSION

Uncertainty Analysis Estimates

The calm water resistance, heave, trim, and model speed experimental values (*D*) were averaged across the test runs for each test condition. Total uncertainty (*U*) values were derived from the experimental precision uncertainty (*P*) and the estimated bias uncertainty (*B*) following the Coleman and Steele approach with the degrees of freedom (DoF) (ν) as described in reference [2]. The degrees of freedom used in this approach is taken as one less than the number of independent test runs (i.e. $\nu = N_{runs} - 1$).

The uncertainties were estimated at a 95% confidence level, giving a 95% probability that the true mean value lies within the reported confidence interval (i.e. $\mu_{true} = (D - U, D + U)$). The precision (or random) uncertainty quantifies the repeatability of the measurement. Precision uncertainties were calculated using the end-to-end method described [2]. The bias uncertainty is the fixed component of the total uncertainty and is also referred to as systematic uncertainty. The total uncertainty was the root sum square of the bias and precision uncertainties. Ideally, both the bias and precision uncertainty should contribute equally to the total uncertainty and the total uncertainty value should be small compared to the measured value. An imbalance of bias or precision uncertainty shows the area for future experimental improvement whether in the equipment or experimental procedure. Further details on the uncertainty analysis can be found in APPENDIX C:.

Mass Properties

The model mass properties were measured using the process described in Appendix B. Table 4 shows the values and uncertainties for model mass properties relevant to calm water performance. Uncertainties were calculated via the methods prescribed in Coleman and Steele [2], A detailed description of the uncertainty calculations is included in APPENDIX C:.

Table 4. Uncertainty in As-Tested Mass Properties

Description	As-Tested Value, *D*	Total Uncertainty, *U*	*U* as %*D*
Displacement, Δ (lbf)	858.00	0.30	0.035%
LCG (inch +FAP)	96.024	0.082	0.085%
VCG (inch +ABL)	9.74	0.38	3.9%
Pitch Mass Moment of Inertia, $I_{y,CG}$ (lbf-ft^2 about CG)	18,536	339	1.8%
Pitch Radius of Gyration, $k_{y,CG}$ (inch about CG)	55.78	0.51	0.91%

Resistance

Resistance is calculated from force measurements at two locations, forward and aft. The equation to calculate total resistance (R_t) for this experiment is:

$$R_t = F_{xfwd} + F_{xaft}\cos(\tau) + F_{zaft}\sin(\tau) \tag{1}$$

where F_{xfwd} is the resistance measured at forward dynamometer, located between the tow post and the pivot,

F_{xaft} is the longitudinal force measured at aft dynamometer, located between the grasshopper restraint and the deck edge,

F_{zaft} is the vertical force measured at aft dynamometer, located between the grasshopper restraint and the deck edge, and

τ is the running trim angle (or change in trim angle from the static floating condition).

The forward dynamometer is located above the model pivot point, so the direction is earth-fixed. The aft dynamometer is mounted to the model, so it needs to be corrected to earth-fixed resistance in the *x*-direction.

The equation to calculate the total resistance coefficient (C_T) for this experiment is:

$$C_T = \frac{R_t}{\frac{1}{2}\rho S_0 V^2} \tag{2}$$

where ρ is the density of water in the model basin,

S_0 is the static wetted surface area,

V is the model speed.

The equation to calculate the friction resistance coefficient (C_F) for this experiment is:

$$C_F = \frac{0.075}{\left(\log\left(\frac{VL_{PP}}{\nu}\right) - 2\right)^2} \tag{3}$$

where L_{PP} is the length between perpendiculars,

ν is the kinematic viscosity of water.

The equation to calculate the total resistance coefficient (C_R) for this experiment is:

$$C_R = C_T - C_F\left(\frac{S}{S_0}\right) \tag{4}$$

where S is the dynamic wetted surface area.

Sinkage and Trim

Sinkage and trim are calculated from string potentiometer measurements at two locations, forward and aft. The equation to calculate the running trim angle from initial conditions is:

$$\tau = \text{asin}\left(\frac{\sigma_{FSP} - \sigma_{ASP}}{L_{SP}}\right) \tag{5}$$

where σ_{FSP} is the sinkage at forward string potentiometer,

σ_{ASP} is the sinkage at aft string potentiometer, and

L_{FSP} is the distance between string potentiometers.

The locations and variables are shown in the sketch in Figure 6 (initial condition) and Figure 7 (with trim). Values of x are positive forward, and trim is positive bow up. The values for these variables are shown in Table 5.

The data reduction equation for the sinkage at the tow point (σ_{TP}) from initial conditions is:

$$\sigma_{TP} = \sigma_{ASP} + X_{TP}\left(\frac{\sigma_{FSP} - \sigma_{ASP}}{L_{SP}}\right) \tag{6}$$

where X_{TP} is the *x* position of tow point measured along the baseline with positive values forward of the aft potentiometer. The values for these variables are shown in Table 5. Tow post sinkage is measured from the initial static waterline with positive values upwards.

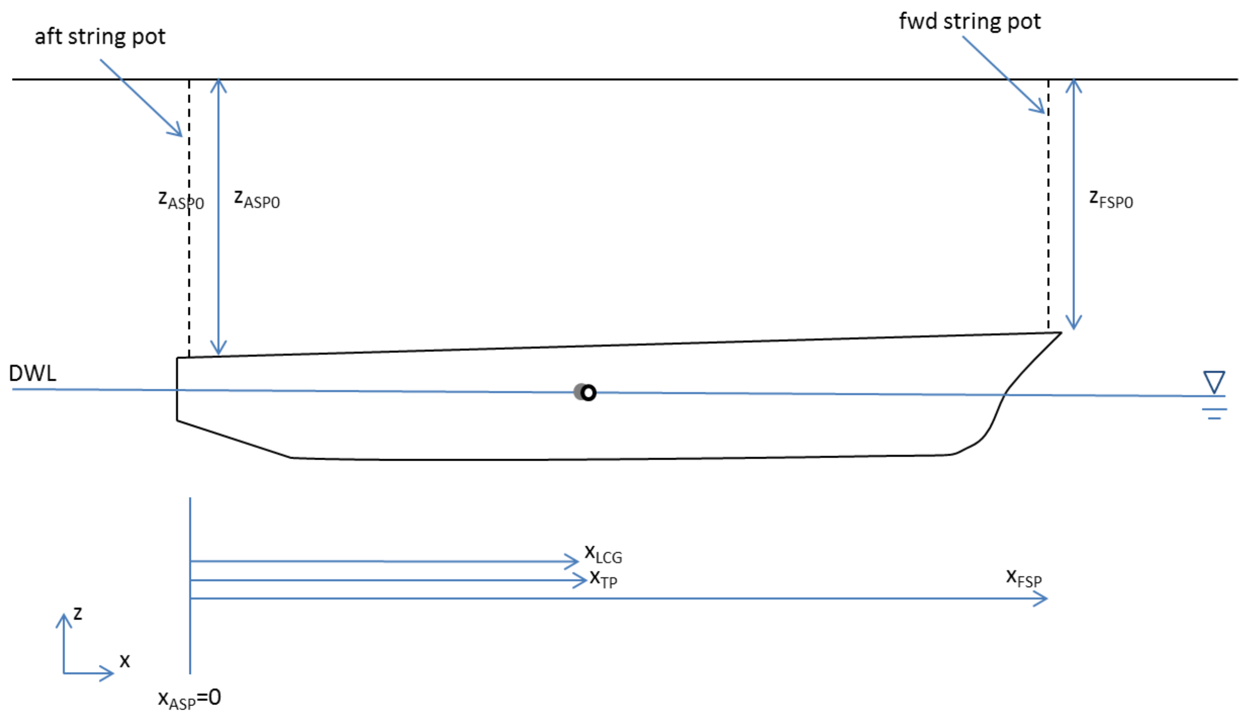

Figure 6. Sketch of *Athena* Model with String Potentiometers in Initial Condition (Not to Scale, Hull Geometry is Notional)

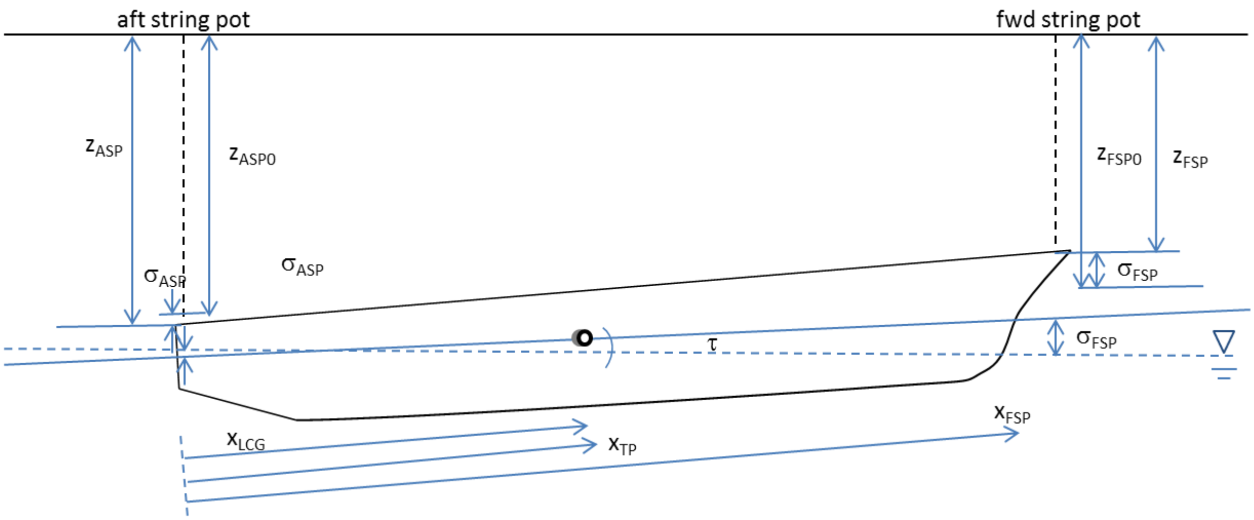

Figure 7. Sketch of Trimmed *Athena* Model with String Potentiometers (Not to Scale, Hull Geometry is Notional)

Table 5. Values for String Potentiometer Positions

Description	As-Tested Value, *D*	Total Uncertainty, *U*	*U* as %*D*
Forward string pot, X_{FSP} (inch +fwd of aft string pot)	237.46	0.036	0.015%
Aft string pot, X_{ASP} (inch +fwd of aft string pot)	0.00	0.036	-
Distance between string pots, L_{SP} (inch)	237.46	0.036	0.015%
LCG position from aft string pot, X_{LCG} (inch +fwd of aft string pot)	96.024	0.079	0.080%
Tow post position from aft string pot, X_{TP} (inch +fwd of aft string pot)	97.381	0.063	0.062%

Table 6 to Table 11 summarize the results of the resistance, sinkage and trim calculations, along with their bias (*B*), precision (*P*), and total (*U*) uncertainties (described in Appendix D). Averages and uncertainties for carriage speed are also included (Table 12). The breakdown of bias uncertainties for each variable in the data reduction equations are also shown in the tables. The contribution of each uncertainty component is shown either as a fraction of total bias uncertainty (for individual bias uncertainties) or total uncertainty (for total combined bias and precision uncertainties).

Figure 10 shows a trim angle comparison between the IMU trim angle measurements and the trim angle calculated from the string potentiometers. These two measurements follow the same trend, but with a constant IMU trim angle offset of approximately 0.4 degrees less than the string potentiometer calculated trim angle. This difference was consistent with IMU installation offsets measured using a handheld inclinometer and the average IMU trim angle for all the runs in a static floating conditions.

In the 2014 test [1], the precision (random) uncertainties are greater than the bias (systematic) uncertainties for nearly all resistance, sinkage, and trim measurements. For this 2015 test, the bias uncertainties for resistance and sinkage has the dominant contribution to total uncertainties, showing improved repeatability in this 2015 test over the previous test in 2014. This improvement is due to the longer settling times between runs. Ideally, both the bias and precision uncertainty should contribute equally to the total uncertainty. Therefore, future reductions in bias errors should follow the reduction in precision error achieved in the 2015 test. Total trim uncertainties ($U\tau$) for this 2015 test are dominated by precision uncertainties ($P\tau$), but smaller than the precision uncertainties for the 2014 test. Also, relative total trim uncertainties ($\%U\tau/D\tau$) are about 1% or less at higher speeds. The small bias uncertainties for trim (i.e. $P\tau >> B\tau$) are attributed to the very small bias sensitivity coefficients ($\theta_{\sigma_{FSP}}, \theta_{\sigma_{ASP}}, \theta_{L_{SP}},$) that are proportional to reciprocal of potentiometer separation distance (i.e. $B_\tau \propto 1/L_{SP}$). This small bias sensitivity is analogous to a long pendulum length (similar to the model's long potentiometer separation) providing high angular resolution.

Dynamic Wetted Hull Surface Area

Underwater photographs and above water video of the dynamic wetted hull surface area were collected at each carriage speed condition. All of the underwater photographs suffered from poor lighting due to the 20 foot depth where the lights and cameras were staged. Determination of the running waterline was also hindered by the underwater viewing location. The running waterline in the mid and after body was above the bilge radius and generally located along the wall sided freeboard. This waterline location could not be determined using the limited perspective of the underwater view. Above water profile video provided an additional method for locating the running waterline and determining the dynamic wetted hull surface area. The running waterline location could be observed well at speeds of 6.3 knots and below as shown in Figure 8. At higher speeds, the running waterline in the fore body was obscured by the bow spray sheet as shown in Figure 9. The above water profile videos that did not have the waterline obscured by the spray sheet were not analyzed to determination of wetted surface area. This dynamic wetted surface area was estimated from the 3D model assuming a straight waterline and using the measured sinkage and trim at each speed.

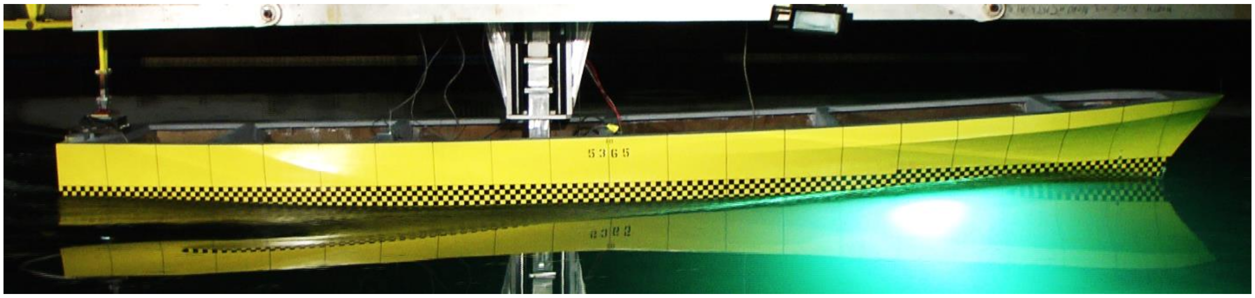

Figure 8. Running Waterline at 6.3 knots (Fr=0.43)

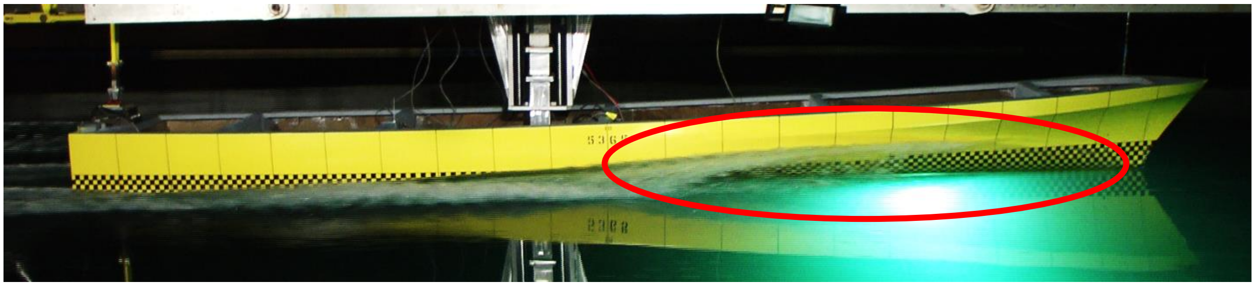

Figure 9. Running Waterline and Bow Spray Sheet at 14.5 knots (Fr=1.00)

Table 6. Uncertainty and Values for Resistance Calculations

Resistance (lbf)	2.09 kts		3.13 kts		3.66 kts		4.18 kts		5.22 kts		6.27 kts		7.66 kts		8.98 kts		10.44 kts		12.19 kts		14.51 kts	
	value	%B	value	%B	value	%B	value	%B	value	%B	value	%B	value	%B	value	%B	value	%B	value	%B	value	%B
$B^2_{Fxfwd}\theta^2_{Fxfwd}$	6.76E-02	58.3%	6.76E-02	58.3%	6.76E-02	58.3%	6.76E-02	58.3%	6.76E-02	58.3%	6.76E-02	58.3%	6.76E-02	58.3%	6.76E-02	58.3%	6.76E-02	58.3%	6.76E-02	58.3%	6.76E-02	58.3%
$B^2_{Fxaft}\theta^2_{Fxaft}$	4.84E-02	41.7%	4.84E-02	41.7%	4.84E-02	41.7%	4.84E-02	41.7%	4.84E-02	41.7%	4.84E-02	41.7%	4.84E-02	41.7%	4.84E-02	41.7%	4.84E-02	41.7%	4.84E-02	41.7%	4.84E-02	41.7%
$B^2_{Fyaft}\theta^2_{Fyaft}$	7.03E-10	0.0%	5.21E-13	0.0%	2.77E-09	0.0%	3.31E-08	0.0%	2.54E-07	0.0%	6.49E-06	0.0%	2.59E-05	0.0%	3.29E-05	0.0%	3.15E-05	0.0%	3.01E-05	0.0%	1.77E-05	0.0%
$B^2_{\tau}\theta^2_{\tau}$	2.60E-11	0.0%	1.09E-10	0.0%	1.32E-09	0.0%	1.01E-09	0.0%	4.72E-10	0.0%	1.63E-09	0.0%	1.74E-09	0.0%	4.28E-09	0.0%	1.43E-09	0.0%	7.16E-10	0.0%	9.50E-11	0.0%
	value	%U	value	%U	value	%U	value	%U	value	%U	value	%U	value	%U	value	%U	value	%U	value	%U	value	%U
B_R	3.41E-01	99.0%	3.41E-01	95.8%	3.41E-01	87.3%	3.41E-01	96.1%	3.41E-01	96.6%	3.41E-01	88.6%	3.41E-01	91.3%	3.41E-01	80.3%	3.41E-01	94.0%	3.41E-01	63.4%	3.41E-01	84.5%
P_R	3.41E-02	1.0%	7.12E-02	4.2%	1.30E-01	12.7%	6.86E-02	3.9%	6.38E-02	3.4%	1.22E-01	11.4%	1.05E-01	8.7%	1.69E-01	19.7%	8.58E-02	6.0%	2.59E-01	36.6%	1.46E-01	15.5%
ν	8		8		7		9		11		7		10		9		11		9		11	
U_R	0.3		0.3		0.4		0.3		0.3		0.4		0.4		0.4		0.4		0.4		0.4	
D	3.0		7.1		10.0		13.1		19.3		30.4		44.5		54.4		65.6		81.0		106.4	
%U/D	11%		5%		4%		3%		2%		1%		1%		1%		1%		1%		0%	

Table 7. Uncertainty and Values for Total Resistance Coefficient Calculations

Total Resistance Coefficient	2.09 kts		3.13 kts		3.66 kts		4.18 kts		5.22 kts		6.27 kts		7.66 kts		8.98 kts		10.44 kts		12.19 kts		14.51 kts	
	value	%B	value	%B	value	%B	value	%B	value	%B	value	%B	value	%B	value	%B	value	%B	value	%B	value	%B
$B^2_S\theta^2_S$	1.04E-09	0.3%	1.16E-09	1.5%	1.23E-09	2.7%	1.26E-09	5.0%	1.12E-09	10.2%	1.34E-09	20.5%	1.29E-09	36.4%	1.03E-09	36.8%	8.08E-10	55.4%	6.69E-10	51.1%	5.71E-10	74.6%
$B^2_V\theta^2_V$	4.08E-10	0.1%	4.05E-10	0.5%	3.93E-10	0.9%	6.21E-11	0.2%	7.95E-11	0.7%	3.61E-11	0.6%	1.67E-11	0.5%	3.94E-10	14.1%	1.91E-11	1.3%	1.26E-10	9.7%	2.06E-12	0.3%
$B^2_{Rt}\theta^2_{Rt}$	3.68E-07	99.6%	7.53E-08	97.9%	4.45E-08	96.5%	2.38E-08	94.7%	9.74E-09	89.0%	5.13E-09	78.7%	2.23E-09	62.8%	1.36E-09	48.7%	6.24E-10	42.8%	5.07E-10	38.8%	1.87E-10	24.5%
$B^2_{\rho}\theta^2_{\rho}$	9.28E-12	0.0%	1.04E-11	0.0%	1.10E-11	0.0%	1.12E-11	0.0%	9.98E-12	0.1%	1.19E-11	0.2%	1.15E-11	0.3%	9.17E-12	0.3%	7.21E-12	0.5%	5.97E-12	0.5%	5.10E-12	0.7%
	value	%U	value	%U	value	%U	value	%U	value	%U	value	%U	value	%U	value	%U	value	%U	value	%U	value	%U
B_{CT}	6.08E-04	99.1%	2.77E-04	96.0%	2.15E-04	93.1%	1.59E-04	97.2%	1.05E-04	96.7%	8.07E-05	92.5%	5.96E-05	95.0%	5.28E-05	97.6%	3.82E-05	97.0%	3.62E-05	93.7%	2.77E-05	95.9%
P_{CT}	5.94E-05	0.9%	5.68E-05	4.0%	5.83E-05	6.9%	2.71E-05	2.8%	1.93E-05	3.3%	2.31E-05	7.5%	1.36E-05	5.0%	8.34E-06	2.4%	6.77E-06	3.0%	9.42E-06	6.3%	5.75E-06	4.1%
U_{CT}	6.11E-04		2.83E-04		2.23E-04		1.61E-04		1.06E-04		8.39E-05		6.11E-05		5.35E-05		3.88E-05		3.74E-05		2.83E-05	
D	5.35E-03		5.66E-03		5.83E-03		5.89E-03		5.55E-03		6.07E-03		5.97E-03		5.32E-03		4.72E-03		4.30E-03		3.97E-03	
%U/D	11.4%		5.0%		3.8%		2.7%		1.9%		1.4%		1.0%		1.0%		0.8%		0.9%		0.7%	

Table 8. Uncertainty and Values for Friction Resistance Coefficient Calculations

Friction Resistance Coefficient																						
	2.09 kts		*3.13 kts*		*3.66 kts*		*4.18 kts*		*5.22 kts*		*6.27 kts*		*7.66 kts*		*8.98 kts*		*10.44 kts*		*12.19 kts*		*14.51 kts*	
	value	*%B*	*value*	*%B*	*value*	*%B*	*value*	*%B*	*value*	*%B*	*value*	*%B*	*value*	*%B*	*value*	*%B*	*value*	*%B*	*value*	*%B*	*value*	*%B*
$B^2_V\theta^2_V$	1.21E-12	7.6%	8.61E-13	6.7%	7.28E-13	6.2%	1.05E-13	1.0%	1.36E-13	1.5%	4.71E-14	0.6%	2.05E-14	0.3%	5.62E-13	7.4%	3.22E-14	0.5%	2.40E-13	3.8%	4.22E-15	0.1%
$B^2_L\theta^2_L$	8.75E-15	0.1%	7.06E-15	0.1%	6.51E-15	0.1%	6.08E-15	0.1%	5.44E-15	0.1%	4.97E-15	0.1%	4.51E-15	0.1%	4.18E-15	0.1%	3.88E-15	0.1%	3.62E-15	0.1%	3.33E-15	0.1%
$B^2_\nu\theta^2_\nu$	1.48E-11	92.4%	1.19E-11	93.2%	1.10E-11	93.7%	1.03E-11	98.9%	9.17E-12	98.5%	8.38E-12	99.4%	7.60E-12	99.7%	7.05E-12	92.6%	6.55E-12	99.5%	6.10E-12	96.2%	5.62E-12	99.9%
	value		*value*		*value*		*value*		*value*		*value*		*value*		*value*		*value*		*value*		*value*	
U_{CF}	4.00E-06		3.57E-06		3.42E-06		3.22E-06		3.05E-06		2.90E-06		2.76E-06		2.76E-06		2.57E-06		2.52E-06		2.37E-06	
D	3.23E-03		3.01E-03		2.93E-03		2.86E-03		2.76E-03		2.67E-03		2.59E-03		2.52E-03		2.46E-03		2.41E-03		2.34E-03	
%U/D	0.1%		0.1%		0.1%		0.1%		0.1%		0.1%		0.1%		0.1%		0.1%		0.1%		0.1%	

Table 9. Uncertainty and Values for Residuary Resistance Coefficient Calculations

Residuary Resistance Coefficient																						
	2.09 kts		*3.13 kts*		*3.66 kts*		*4.18 kts*		*5.22 kts*		*6.27 kts*		*7.66 kts*		*8.98 kts*		*10.44 kts*		*12.19 kts*		*14.51 kts*	
	value	*%B*	*value*	*%B*	*value*	*%B*	*value*	*%B*	*value*	*%B*	*value*	*%B*	*value*	*%B*	*value*	*%B*	*value*	*%B*	*value*	*%B*	*value*	*%B*
$B^2_{CT}\theta^2_{CT}$	3.73E-07	99.8%	8.02E-08	99.2%	4.95E-08	98.7%	2.59E-08	97.7%	1.13E-08	95.1%	7.04E-09	92.7%	3.74E-09	87.9%	2.86E-09	85.6%	1.50E-09	77.0%	1.40E-09	76.5%	7.99E-10	66.8%
$B^2_{CF}\theta^2_{CF}$	1.61E-11	0.0%	1.31E-11	0.0%	1.21E-11	0.0%	1.08E-11	0.0%	9.98E-12	0.1%	9.28E-12	0.1%	8.24E-12	0.2%	7.93E-12	0.2%	6.64E-12	0.3%	6.41E-12	0.4%	5.46E-12	0.5%
$B^2_S\theta^2_S$	3.78E-10	0.1%	3.27E-10	0.4%	3.10E-10	0.6%	2.97E-10	1.1%	2.75E-10	2.3%	2.59E-10	3.4%	2.43E-10	5.7%	2.31E-10	6.9%	2.20E-10	11.3%	2.10E-10	11.5%	1.99E-10	16.6%
$B^2_{S0}\theta^2_{S0}$	3.82E-10	0.1%	3.36E-10	0.4%	3.21E-10	0.6%	3.09E-10	1.2%	2.95E-10	2.5%	2.85E-10	3.8%	2.63E-10	6.2%	2.41E-10	7.2%	2.22E-10	11.4%	2.12E-10	11.6%	1.93E-10	16.1%
	value		*value*		*value*		*value*		*value*		*value*		*value*		*value*		*value*		*value*		*value*	
U_{CR}	6.12E-04		2.84E-04		2.24E-04		1.63E-04		1.09E-04		8.72E-05		6.52E-05		5.78E-05		4.42E-05		4.27E-05		3.46E-05	
D	2.11E-03		2.62E-03		2.86E-03		2.97E-03		2.70E-03		3.27E-03		3.27E-03		2.75E-03		2.25E-03		1.88E-03		1.66E-03	
%U/D	29.0%		10.8%		7.8%		5.5%		4.0%		2.7%		2.0%		2.1%		2.0%		2.3%		2.1%	

Table 10. Uncertainty and Values for Trim Calculations

Trim (deg)	2.09 kts		3.13 kts		3.66 kts		4.18 kts		5.22 kts		6.27 kts		7.66 kts		8.98 kts		10.44 kts		12.19 kts		14.51 kts	
	value	%B	value	%B	value	%B	value	%B	value	%B	value	%B	value	%B	value	%B	value	%B	value	%B	value	%B
$B^2_{\sigma FSP}\theta^2_{\sigma FSP}$	2.84E-08	20.0%	2.84E-08	20.0%	2.84E-08	20.0%	2.84E-08	20.0%	2.84E-08	20.0%	2.84E-08	20.0%	2.84E-08	20.0%	2.84E-08	20.0%	2.84E-08	20.0%	2.84E-08	20.0%	2.84E-08	20.0%
$B^2_{\sigma ASP}\theta^2_{\sigma ASP}$	1.14E-07	80.0%	1.14E-07	80.0%	1.14E-07	80.0%	1.14E-07	80.0%	1.14E-07	80.0%	1.14E-07	80.0%	1.14E-07	80.0%	1.14E-07	80.0%	1.14E-07	80.0%	1.14E-07	80.0%	1.14E-07	80.0%
$B^2_{LSP}\theta^2_{LSP}$	2.07E-16	0.0%	1.53E-19	0.0%	8.16E-16	0.0%	9.74E-15	0.0%	7.48E-14	0.0%	1.91E-12	0.0%	7.64E-12	0.0%	9.68E-12	0.0%	9.29E-12	0.0%	8.88E-12	0.0%	5.22E-12	0.0%
	value	%U	value	%U	value	%U	value	%U	value	%U	value	%U	value	%U	value	%U	value	%U	value	%U	value	%U
B_τ	0.0004	4.1%	0.0004	0.5%	0.0004	2.1%	0.0004	2.3%	0.0004	1.4%	0.0004	0.4%	0.0004	0.3%	0.0004	0.3%	0.0004	0.8%	0.0004	0.4%	0.0004	0.2%
P_τ	0.0018	95.9%	0.0034	98.8%	0.0026	97.9%	0.0024	97.7%	0.0031	98.6%	0.0060	99.6%	0.0067	99.7%	0.0072	99.7%	0.0042	99.2%	0.0058	99.6%	0.0079	99.8%
ν	8		8		7		9		11		7		10		9		11		9		11	
U_τ	0.0019		0.0035		0.0026		0.0025		0.0031		0.0060		0.0067		0.0072		0.0042		0.0059		0.0080	
D	-0.0054		-0.0001		0.0108		0.0372		0.1031		0.5211		1.0423		1.1731		1.1490		1.1233		0.8614	
%U/D	-34.4%		n/a		24.2%		6.6%		3.0%		1.1%		0.6%		0.6%		0.4%		0.5%		0.9%	

Table 11. Uncertainty and Values for Sinkage at Tow Point Calculations

Sinkage LTP (in)	2.09 kts		3.13 kts		3.66 kts		4.18 kts		5.22 kts		6.27 kts		7.66 kts		8.98 kts		10.44 kts		12.19 kts		14.51 kts	
	value	%B	value	%B	value	%B	value	%B	value	%B	value	%B	value	%B	value	%B	value	%B	value	%B	value	%B
$B^2_{\sigma FSP}\theta^2_{\sigma FSP}$	2.69E-04	10.8%	2.69E-04	10.8%	2.69E-04	10.8%	2.69E-04	10.8%	2.69E-04	10.8%	2.69E-04	10.8%	2.69E-04	10.8%	2.69E-04	10.8%	2.69E-04	10.8%	2.69E-04	10.8%	2.69E-04	10.8%
$B^2_{\sigma ASP}\theta^2_{\sigma ASP}$	2.23E-03	89.2%	2.23E-03	89.2%	2.23E-03	89.2%	2.23E-03	89.2%	2.23E-03	89.2%	2.23E-03	89.2%	2.23E-03	89.2%	2.23E-03	89.2%	2.23E-03	89.2%	2.23E-03	89.2%	2.23E-03	89.2%
$B^2_{LSP}\theta^2_{LSP}$	2.41E-12	0.0%	1.79E-15	0.0%	9.51E-12	0.0%	1.13E-10	0.0%	8.72E-10	0.0%	2.23E-08	0.0%	8.90E-08	0.0%	1.13E-07	0.0%	1.08E-07	0.0%	1.03E-07	0.0%	6.08E-08	0.0%
	value	%U	value	%U	value	%U	value	%U	value	%U	value	%U	value	%U	value	%U	value	%U	value	%U	value	%U
B_σ	0.05	88.6%	0.05	88.3%	0.05	82.4%	0.05	78.5%	0.05	77.7%	0.05	72.3%	0.05	86.9%	0.05	91.2%	0.05	89.8%	0.05	91.4%	0.05	73.4%
P_σ	0.02	11.4%	0.02	11.7%	0.02	17.6%	0.03	21.5%	0.03	22.3%	0.03	27.7%	0.02	13.1%	0.02	8.8%	0.02	10.2%	0.02	8.6%	0.03	26.6%
ν	8		8		7		9		11		7		10		9		11		9		11	
U_σ	0.05		0.05		0.06		0.06		0.06		0.06		0.05		0.05		0.05		0.05		0.06	
D	-0.1		-0.2		-0.2		-0.3		-0.5		-0.8		-0.8		-0.5		-0.3		-0.2		0.0	
%U/D	n/a		33%		25%		20%		12%		8%		7%		10%		18%		34%		308%	

Table 12. Uncertainty and Values for Carriage Speed

	2.09 kts		*3.13 kts*		*3.66 kts*		*4.18 kts*		*5.22 kts*		*6.27 kts*		*7.66 kts*		*8.98 kts*		*10.44 kts*		*12.19 kts*		*14.51 kts*	
	value	*%U*	*value*	*%U*	*value*	*%U*	*value*	*%U*	*value*	*%U*	*value*	*%U*	*value*	*%U*	*value*	*%U*	*value*	*%U*	*value*	*%U*	*value*	*%U*
B_s	3.15E-04	1%	3.15E-04	0%	3.15E-04	0%	3.15E-04	1%	3.15E-04	1%	3.15E-04	1%	3.15E-04	1%	3.15E-04	0%	3.15E-04	0%	3.15E-04	0%	3.15E-04	1%
P_s	0.00	99%	0.01	100%	0.01	100%	0.00	99%	0.00	99%	0.00	99%	0.00	99%	0.02	100%	0.00	100%	0.02	100%	0.00	99%
v	8		8		7		9		11		7		10		9		11		9		11	
U_s	0.00	100%	0.01	100%	0.01	100%	0.00	100%	0.00	100%	0.00	100%	0.00	100%	0.02	100%	0.00	100%	0.02	100%	0.00	100%
D	2.1		3.1		3.7		4.2		5.2		6.3		7.7		9.0		10.5		12.2		14.5	
%U/D	0.2%		0.2%		0.2%		0.1%		0.1%		0.0%		0.0%		0.2%		0.0%		0.1%		0.0%	

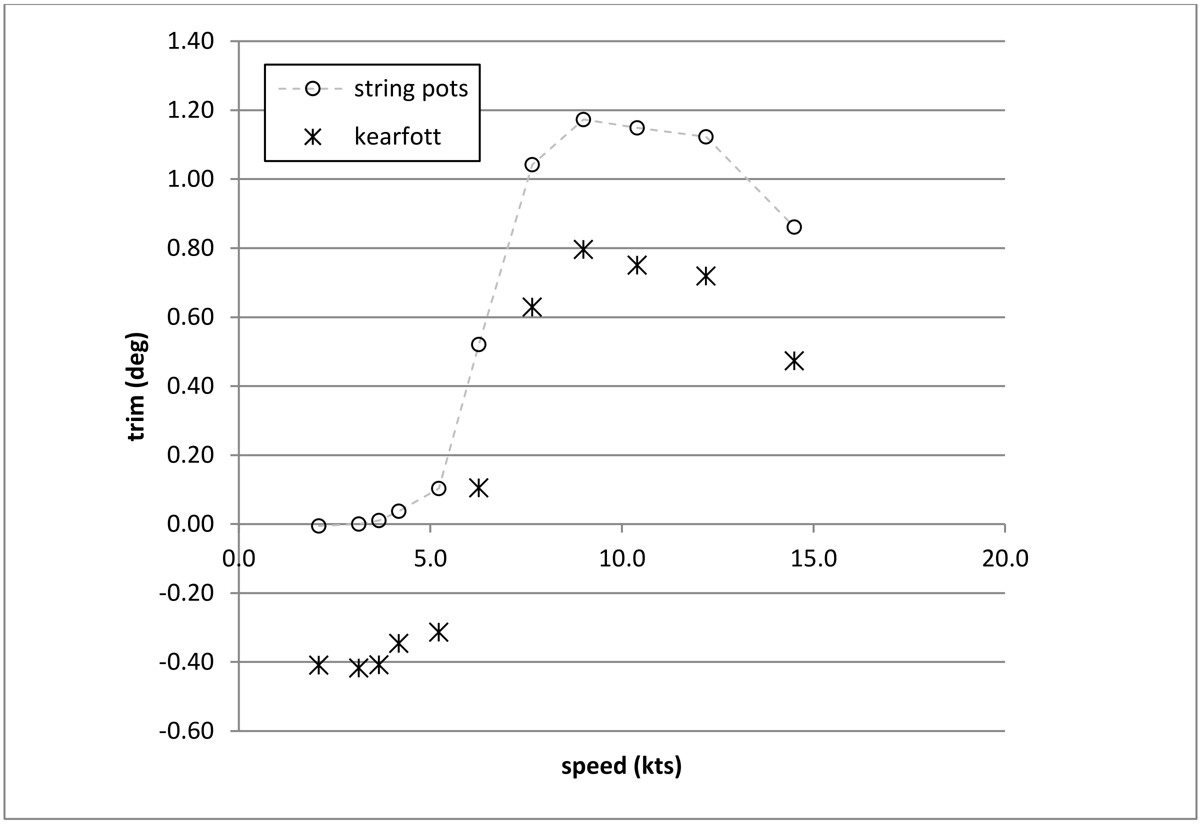

Figure 10. Trim Comparison of String Potentiometer Calculations and IMU (Kearfott) Measurements

CONCLUSIONS

A detailed uncertainty analysis was performed on the data collected for this test, providing a complete calm water data set for CFD predictions and comparisons. Uncertainty estimates for resistance and trim are small, while uncertainty measurements for sinkage are larger. The applied lessons learned from previous testing [1] (longer basin settling times) appeared to reduce the precision uncertainty in this 2015 test. Even longer test runs and longer settling times may help further reduce sinkage uncertainty for future testing, if necessary. The unbalanced bias and precision uncertainties for trim (i.e. $P\tau >> B\tau$) are considered acceptable since the total trim uncertainty is small.

The translation of the tow point allows for a more accurate representation of full scale motions. At full scale, the craft would pitch about the center of gravity and moving the tow point to the center of gravity allows the model to pitch about the center of gravity. Moving the tow point also eliminates the uncertainty of the complex motion of the model in CFD simulations when towed from the 2014 tow point.

RECOMMENDATIONS

The methods for determining the location of the running waterline and determination of the dynamic wetted surface area could be improved if frictional and residuary components of resistance at full scale are an important test objective. Underwater photographs that are extracted from video need a significant amount of lighting (intensity and number of lights). There is a tradeoff between the ease of staging underwater fixtures directly on the basin bottom and the reduced lighting needs when staging is constructed at a lower depth. During this test, numerous lights were necessary to illuminate the underwater hull thru 20 feet of water. This only provided minimally acceptable hull illumination; limited the video and photograph resolution; and significantly loaded the electrical breaker panels supplying power to the underwater lights. This issue could be mitigated if available time and resources were available to better optimize the underwater staging; and using lower power, high intensity, LED lights suitable for underwater operation.

Additional above water cameras could be strategically placed on the carriage to observe the separation of the bow spray sheet from the hull surface. Several trial runs would be needed to identify the hull location to focus a camera and where a camera could be secured to the underside of the carriage.

REFERENCES

[1] Fullerton, A., Geiser, J., Punzi, S., Morin, J., Weil, C., Walker, D., Lee, E., Jiang, M., Lien, V., and Merrill, C., "Assessment of Hydrodynamic and Structural Analysis Tools for *R/V Athena* in Calm Water," Naval Surface Warfare Center, Carderock Division, Naval Architecture and Engineering Department Technical Report, NSWCCD-80-TR-2019/035, November 2019.

[2] Coleman, H. and W. G. Steele. *Experimentation and Uncertainty Analysis for Engineers,* Second Edition, John Wiley and Sons, New York, 1999.

THIS PAGE INTENTIONALLY LEFT BLANK

APPENDIX A: DYNAMOMETER CALIBRATIONS

The dynamometers were assembled at NSWCCD (serial No. 2003-3 and 2003-4) using four Kistler force sensors (Type 9602A3211) capable of measuring force in 3 axes. The sensors were sandwiched between two plates of 1-inch thick heat-treated 17-4 stainless steel and preloaded to the manufacturer's specification. Each of the sensors is evenly spaced around the center of the dynamometer. The voltages were recorded using a computer based data acquisition system. The dynamometer assembly was shown in Figure A - 1.

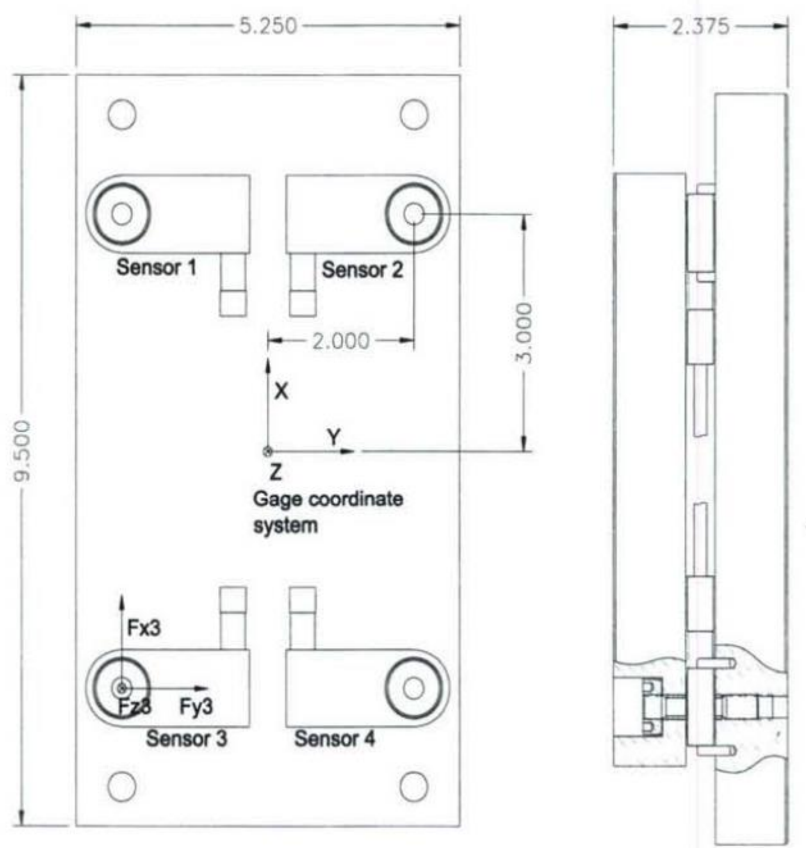

Figure A - 1. Dynamometer Assembly

To calibrate the dynamometer, NIST traceable calibration weights were hung from dynamometer using a calibration fixture with known, fixed moment arms. The input load and the output voltages were recorded for each calibration point. Each axis was loaded in force and moment independently for a total of approximately 140 calibration points. The measurements were averaged for 3 seconds at 100 Hz. The forces and moments on the dynamometer assembly were calculated using equations A-1 through A-6:

$$Fx_{sum} = Fx1 + Fx2 + Fx3 + Fx4 \quad \text{(A-1)}$$
$$Fy_{sum} = Fy1 + Fy2 + Fy3 + Fy4 \quad \text{(A-2)}$$
$$Fz_{sum} = Fz1 + Fz2 + Fz3 + Fz4 \quad \text{(A-3)}$$
$$Mx_{sum} = Ry * (-Fz1 + Fz2 - Fz3 + Fz4) \quad \text{(A-4)}$$
$$My_{sum} = Rx * (-Fz1 - Fz2 + Fz3 + Fz4) \quad \text{(A-5)}$$
$$Mz_{sum} = Ry * (Fx1 - Fx2 + Fx3 - Fx4) + Rx * (Fy1 + Fy2 - Fy3 - Fy4) \quad \text{(A-6)}$$

where N is the gage number, N=1,2,3,4,

FxN is the input load in X gage direction from gage N,

FyN is the input load in Y gage direction from gage N,

FzN is the input load in Z gage direction from gage N,

Rx and Ry are the moment arms between the gages and dynamometer coordinate systems,

Fx_{sum} is the sum of forces in X dynamometer direction,

Fy_{sum} is the sum of forces in Y dynamometer direction,

Fz_{sum} is the sum of forces in Z dynamometer direction,

Mx_{sum} is the sum of moments about the X dynamometer axis,

My_{sum} is the sum of moments about the Y dynamometer axis, and

Mz_{sum} is the sum of moments about the Z dynamometer axis.

The input loads and the above calculated forces and moments were used to generate an interaction matrix (A^{-1}) that minimizes the regression errors, using pseudo inverse technique as shown below.

$$A^{-1} = ((F^T * F)^{-1} * F^T * F_{sum})^{-1} \quad \text{(A-7)}$$

where F_{sum} is the (6 x N) matrix containing the force and moment outputs as dynamometer voltage signals, and

F is the (6 x N) matrix containing the applied, or calibration, loads (forces and moments).

Equation A-8 is then used to derive an applied loads from the dynamometer voltage signals.

$$F = F_{sum} * A^{-1} \quad \text{(A-8)}$$

The calibration errors can then be estimated using equation A-9.

$$Error = F - F_{sum} * A \quad \text{(A-9)}$$

The dynamometers were calibrated before and after the test. Table A - 1 and Table A - 2 show the interaction matrix for each dynamometer. Table A - 3 and Table A - 4 below summarize the post-test calibration results of each dynamometer. The bias uncertainties at a 95% confidence level in surge and sway were estimated using the calibration error standard deviation given in the table (95% Confidence Interval = 2*s). The surge and sway bias uncertainties for the forward tow post dynamometer were B_{Fxfwd}=0.26 lbf and B_{Fyfwd}=0.16 lbf respectively. The surge and sway bias uncertainties for the aft grasshopper dynamometer were B_{Fxaft}=0.22 lbf and B_{Fyaft}=0.28 lbf respectively. These bias uncertainties in the component directions for each dynamometer were used estimate the total resistance uncertainty.

Table A - 1. Tow Post Dynamometer (S/N 2003-3) Interaction Matrix

	$F_{x_{sum}}$	$F_{y_{sum}}$	$F_{z_{sum}}$	$M_{x_{sum}}$	$M_{y_{sum}}$	$M_{z_{sum}}$
F_x	0.94865	-0.00020	-0.00095	0.00148	-0.00611	0.00361
F_y	-0.00067	0.94155	-0.00055	0.00416	-0.00302	0.00254
F_z	0.00421	0.00341	1.00305	-0.00105	0.00154	0.00013
M_x	-0.00399	-0.00816	-0.02079	1.01150	-0.01034	0.00208
M_y	-0.00439	-0.00795	0.02572	-0.00459	1.00840	-0.00223
M_z	0.02998	-0.01586	0.01027	0.00030	-0.00287	0.94401

Table A - 2. Aft Grasshopper Dynamometer (S/N 2003-4) Interaction Matrix

	$F_{x_{sum}}$	$F_{y_{sum}}$	$F_{z_{sum}}$	$M_{x_{sum}}$	$M_{y_{sum}}$	$M_{z_{sum}}$
F_x	0.95510	-0.00461	0.00191	-0.00066	-0.00475	0.00096
F_y	0.00182	0.95272	0.00288	0.00463	0.00129	-0.00361
F_z	-0.00231	-0.00168	1.00001	-0.00272	0.00210	-0.00065
M_x	0.00836	0.02485	-0.06573	1.00810	-0.02154	-0.00429
M_y	-0.00479	0.01705	0.03464	-0.01278	1.00389	-0.00072
M_z	0.00968	-0.03093	-0.01844	0.00009	-0.00137	0.96307

Table A - 3. Tow Post Dynamometer (S/N 2003-3) Calibration Results

	Fx (lbf)	Fy (lbf)	Fz (lbf)	Mx (ft-lbf)	My (ft-lbf)	Mz (ft-lbf)
Range	200	100	600	118.75	118.75	50
Max Error (%Range)	0.13 (0.06%)	0.14 (0.14%)	0.44 (0.07%)	0.09 (0.08%)	0.15 (0.13%)	0.22 (0.43%)
Min Error (%Range)	-0.52 (-0.26%)	-0.27 (-0.27%)	-1.39 (-0.23%)	-0.23 (-0.20%)	-0.18 (-0.15%)	-0.08 (-0.17%)
Standard Deviation, s	0.13	0.08	0.28	0.007	0.007	0.011

Table A - 4. Aft Grasshopper Dynamometer (S/N 2003-4) Calibration Results

	Fx (lbf)	Fy (lbf)	Fz (lbf)	Mx (ft-lbf)	My (ft-lbf)	Mz (ft-lbf)
Range	200	100	550	118.75	118.75	50.78125
Max Error (%Range)	0.20 (0.09%)	0.17 (0.17%)	0.80 (0.09%)	0.14 (0.07%)	0.17 (0.13%)	0.09 (1.45%)
Min Error (%Range)	-0.31 (-0.17%)	-0.51 (-0.51%)	-2.32 (-0.42%)	-0.18 (-0.15%)	-0.22 (-0.18%)	-0.08 (-0.17%)
Standard Deviation, s	0.11	0.14	0.35	0.05	0.008	0.022

APPENDIX B: SWINGING PROCEDURE

An inertial frame was used to swing the model for determination of the model mass properties. This inertial frame consists of a steel A-frame with approximate dimensions of 12 feet high, 8.4 feet long, and 8 feet wide. A pivot post suspended from the steel structure was used to support the model as a rigidly connected pendulum. The pivot post was configured with a roller bearing joint and beam fixture that was used to rigidly fasten the model to the A-frame. This A-frame and associated pivot hardware have an approximate capacity for models up to 1,200 pounds, 22 feet long, and 6 feet wide. The A-frame can be readily reconfigured to swing a model about both the roll and pitch axes. The roll and yaw moments of inertia were not measured since the model was only tested in the heave and pitch degrees of freedom. Figure B - 1 shows the model as-configured on the inertial A-frame apparatus. The swinging procedures used to measure the model's mass properties follow the NSWCCD guidance.

Figure B - 1. Model as-swung on the inertial A-frame

The model's mass properties were configured prior to testing to the same values used in the 2014 test. The as-tested mass properties were determined after the test was completed to capture minor model configuration changes that occurred during testing. These configuration changes resulted from rigging constraints on the tow post, instrumentation changes, and refinements in ballast weights to achieve zero hydrostatic heel and trim angles. The tow post gimbal and A-frame pivot were both attached to the onboard mounting plate that was fixed at 97.381 inches forward of the aft perpendicular (FAP). This mounting plate location was not adjustable. The model's ballast weight was shifted to achieve a zero hydrostatic trim angle as indicated by the marked waterline before proceeding with testing. This ballast weight shift moved the as-tested longitudinal center of gravity (LCG=96.024 inches +FAP) aft of the mounting plate center (i.e. longitudinal tow post location, LTP=97.381 inches +FAP). All mass moment of inertia measurements were reported about the as-tested center of gravity.

The as-swung mass properties did not include the as-tested weight components for the carriage tow post and rigging. These component weights were included analytically when deriving the as-tested mass properties. The tow post weight acted as a point load at the gimbal axis of rotation and was assumed to have no moment of inertia contribution to the as-tested moment of inertia.

The model's vertical center of gravity (VCG) was determined via static inclining moments while mounted to the A-frame pivot. This inclining was performed by moving an inclining weight longitudinally and measuring the change in trim angle due to the corresponding moment of the inclining weight. From these values, the model VCG was determined relative to the A-frame pivot and then reported relative to the model baseline. This inclining procedure was performed over a range of angles to establish a suitable linear trend for deriving the as-swung VCG.

The pitch moment of inertia was determined by swinging the model about the A-frame pivot. The swing oscillations were limited to four degrees or less for consistency with the small angle approximation used to solve the differential equation relating mass moment of inertia to the oscillation natural period. The parallel axis theorem was then used determine and report mass moment of inertia about the as-tested center of gravity.

Table B - 1. *Athena* model loading during testing and post-test swinging

Model Loading Component	Value (D)	Total Uncertainty (U)
As-Swung Model Weight (lb)	840.09	0.14
As-Swung Model LCG (inch +FAP)	97.381	0.067
As-Swung Model VCG (inch +ABL)	9.65	0.39
As-Swung Model Pitch Gyradius (inch about CG)	57.22	0.47
As-Tested Tow Post and Rigging Weight (lb)	35.00	0.10
As-Tested Tow Post and Rigging LCG (inch +FAP)	97.381	0.063
As-Tested Tow Post and Rigging VCG (inch +ABL)	10.040	0.063
Removed Trimming Ballast Weight (lb)	17.09	0.10
Removed Trimming Ballast LCG (inch +FAP)	165.506	0.063
Removed Trimming Ballast VCG (inch +ABL)	5.790	0.063
As-Tested Model Weight (lb)	858.00	0.22
As-Tested Model LCG (inch +FAP)	96.024	0.076
As-Tested Model VCG (inch +ABL)	9.74	0.38
As-Tested Model Pitch Gyradius (inch about CG)	55.78	0.51

APPENDIX C: *ATHENA* CALM WATER MODEL TEST – UNCERTAINTY ANALYSIS

CONTENTS

BACKGROUND....C-3
APPROACH....C-7
Total Resistance....C-7
Total Resistance Coefficient....C-8
Friction Resistance Coefficient....C-9
Residuary Resistance Coefficient....C-9
Trim Angle from String Potentiometers....C-10
Sinkage....C-11
Mass Properties....C-12
Weight....C-12
Center of Gravity (CG)....C-13
Vertical Center of Gravity (VCG)....C-14
Longitudinal Center of Gravity (LCG)....C-18
Carriage Speed....C-21
REFERENCES....C-21

FIGURES

Figure C - 1. Inclining Plot of (w_i*d_i/W_{tot}) vs (tan α_i)....C-14

TABLES

Table C - 1. Uncertainties for Resistance Measurement....C-10
Table C - 2. Uncertainties for Trim Measurement....C-11
Table C - 3. Uncertainties for Sinkage Measurement....C-12
Table C - 4. Uncertainties for Instrumentation in Calculation of Model Mass Properties....C-12
Table C - 5. Uncertainty in As-Tested Weight Items....C-13
Table C - 6. Uncertainty for *VCG*: As-Inclined....C-15

Table C - 7. Uncertainty for *VCG1*: As-Inclined Without Inclining Weights C-16
Table C - 8. Uncertainty for VCG'_o: As-Inclined Without Inclining Weights and Support BeamC-17
Table C - 9. Uncertainty for VCG_o: As-Inclined Without Inclining Weights and Support Beam above Baseline C-17
Table C - 10. Uncertainty for *VCG*: As-Tested above Baseline C-18
Table C - 11. Uncertainty for *LCG1*: As-Inclined Without Inclining Weights C-19
Table C - 12. Uncertainty for LCG'_o: As-Inclined Without Inclining Weight and Support Beam............................C-19
Table C - 13. Uncertainty for LCG_o: As-Inclined Without Inclining Weight and Support Beam Forward of Aft Perpendicular C-20
Table C - 14. Uncertainty for *LCG*: As-Tested Forward of Aft Perpendicular C-21
Table C - 15. Uncertainties for Carriage Speed............................C-21

BACKGROUND

A detailed uncertainty analysis of the calm water *Athena* model test data was performed, using the approach outlined in Coleman and Steele [C-1], Chapter 4 and Appendix B. This approach includes the standards issued by the American Society of Mechanical Engineers (ASME) [C-2], revision of [C-3] and the American Institute of Aeronautics and Astronautics (AIAA) [C-4]. This approach adopts the methodology of the International Organization for Standardization (ISO) *Guide to the Expression of Uncertainty in Measurement* [C-5], though the terminology differs, specifically in the categorization of the uncertainties.

Figure C - 1 shows a flow diagram of the propagation of errors into the experimental results. The individual measurement systems (*1, 2,…J*) used in the experiment are influenced by a number of elemental error sources. The elemental errors are made up of a bias, or systematic, ($B_1, B_2, \ldots, BJ$) error and a precision, or random, ($P_1, P_2, \ldots, PJ$) error in the measured value of the variable. The bias error is the fixed or constant component of the total error and is also referred to as systematic error. The precision (or random) error quantifies the repeatability of the measurement. These errors then propagate through the data reduction equation ($r=r(X_1, X2, \ldots X_J)$) and result in a bias (B_r) and precision (P_r) error in the final experimental result.

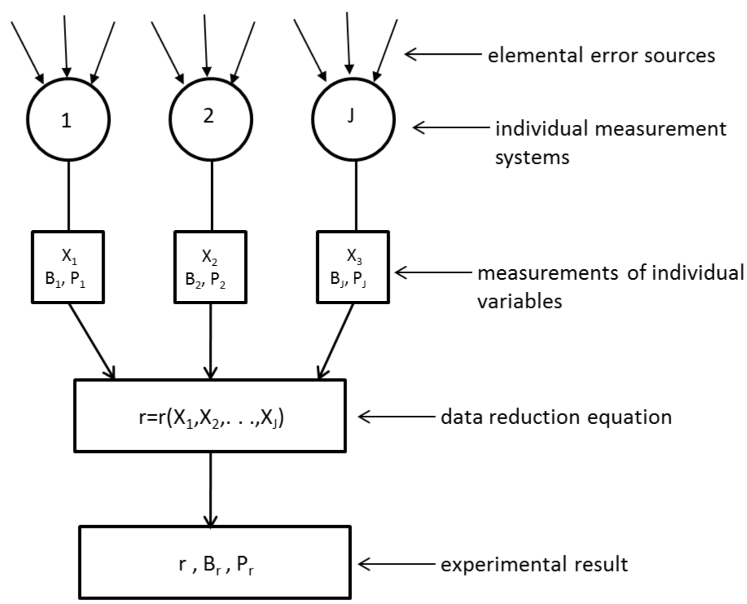

Figure C - 1. Propagation of Errors into an Experimental Result [C-1]

The general data reduction equation is shown in Equation (C-1), where r is the experimental result determined from J measured variables, X_i:

$$r = r(X_1, X_2, \ldots, X_J) \tag{C-1}$$

The total uncertainty is given by:

$$U_r^2 = B_r^2 + P_r^2 \tag{C-2}$$

where U_r is the overall uncertainty, B_r is the bias uncertainty, and P_r is the precision uncertainty.

The bias uncertainty is defined as:

$$B_r^2 = \sum_{i=1}^{J} \theta^2 B_i^2 + 2 \sum_{i=1}^{J-1} \sum_{k=i+1}^{J} \theta_i \theta_j B_{ik} \tag{C-3}$$

where B_i is the bias uncertainty of the measured variables X_i in Equation (C-1), and B_{ik} is the covariance estimator for the systematic errors in X_i and X_k defined as:

$$B_{ik} = \sum_{\alpha=1}^{L} (B_i)_\alpha (B_k)_\alpha \tag{C-4}$$

where L is the number of elemental systematic error sources that are common for measurement of variables X_i and X_k, and θ_i is the sensitivity coefficient, defined as the partial derivative of r with respect to the individual variables X_i:

$$\theta_i = \frac{\partial r}{\partial X_i} \tag{C-5}$$

The precision uncertainty is (assuming no correlated precision errors):

$$P_r^2 = \sum_{i=1}^{J} \theta^2 P_i^2 \tag{C-6}$$

where P_i precision uncertainty of the variables X_i in Equation (C-1). This equation assumes that the instrument uncertainties are independent.

The first step of the uncertainty analysis is to estimate the biases due to elemental errors that affect the individual measurement systems. These biases can include (but are not limited to) calibration errors, data acquisition errors, and conceptual errors. There is no way to calculate bias errors directly; they must always be estimated [C-1]. The approach described here assumes that they are estimated at the 95% confidence interval, consistent with the 95% confidence level used when expanding the precision uncertainty. The total bias error for each measurement system is the root-sum-square (RSS) of the individual bias uncertainties for each variable X_i:

$$B_j = \left[\sum_{k=1}^{M} \left(B_j\right)_k^2 \right]^{1/2} \tag{C-7}$$

Once the bias uncertainties are estimated for each of the measured variables, the total bias (systematic) uncertainty can be determined from Equation (C-3). In cases where the different variables do not share common elemental error sources, the covariance terms are zero, and Equation (C-3) becomes:

$$B_r^2 = \left(\frac{\partial r}{\partial X_1}\right)^2 B_1^2 + \left(\frac{\partial r}{\partial X_2}\right)^2 B_2^2 + \cdots + \left(\frac{\partial r}{\partial X_J}\right)^2 B_J^2 \tag{C-8}$$

or

$$B_r^2 = (\theta_1)^2 B_1^2 + (\theta_2)^2 B_2^2 + \cdots + \left(\theta_J\right)^2 B_J^2 \tag{C-9}$$

The calculation of the precision (random) uncertainty is shown in Equation (C-6), which is the root-sum-square (RSS) of the precision limits for the individual variables multiplied by their sensitivity coefficients. Precision uncertainties are assumed to have a Gaussian distribution, which “has been found to describe more real cases of experimental and instrument variability than any other distribution” [C-1]. The standard deviation (σ_x) and mean (μ_x) of the parent population are typically unknown, so the sample standard deviation and sample mean of one test run (*M*=1) with *N* samples are estimated as follows:

$$s_{x_i} = \left[\frac{1}{N-1}\sum_{i=1}^{N}(X_i - \bar{X}_{M=1})^2\right]^{1/2} \tag{C-10}$$

where the mean is

$$\bar{X}_{M=1} = \frac{1}{N}\sum_{i=1}^{N} X_i \tag{C-11}$$

When there are *j*=1,2,3,…,*M* mean results from *M* separate test runs, the standard deviation of the means ($s_{\bar{x}}$) and the mean of means (or grand mean, $\bar{\bar{X}}$) are the typical descriptive statistics used to evaluate repeatability of multiple runs conducted under the same test conditions, which are defined as follows:

$$s_{\bar{x}} = \frac{s_{x_j}}{\sqrt{M}} \tag{C-12}$$

where

$$s_{x_j} = \left[\frac{1}{M-1}\sum_{j=1}^{M}\left(\bar{X}_j - \bar{\bar{X}}\right)^2\right]^{1/2} \tag{C-12.1}$$

a test run mean is

$$\bar{X}_j = \frac{1}{N}\sum_{i=1}^{N} X_i$$

the grand mean is

$$\bar{\bar{X}} = \frac{1}{M}\sum_{j=1}^{M} \bar{X}_j \tag{C-12.2}$$

The next step is to expand the precision uncertainty to a 95% confidence level. For a Gaussian parent distribution, the standard *z*-score is 1.96 for a population mean 95% confidence interval. For one test run (*M*=1), this is defined as follows:

$$Prob(\bar{X}_{M=1} - 1.96\sigma_x \le \mu_x \le \bar{X}_{M=1} + 1.96\sigma_x) = 0.95 \tag{C-13}$$

For the grand mean calculated from *M* test runs, the 95% confidence interval for the population mean is then estimated as follows:

$$Prob\left(\bar{\bar{X}} - 1.96\frac{\sigma_x}{\sqrt{M}} \le \mu_x \le \bar{\bar{X}} + 1.96\frac{\sigma_x}{\sqrt{M}}\right) = 0.95 \tag{C-14}$$

When the population standard deviation (σ_x) and mean (μ_x) are unknown, the sample standard deviation (s_x) and sample mean ($\bar{X}$) are used to estimate the confidence intervals. The confidence interval for the population mean is estimated using a Student-*t* distribution statistic (*t*) as shown below for one test run (*M*=1) and multiple test runs (*j*=1, 2, 3,…, *M*) respectively:

$$Prob\left(-t \leq \frac{\bar{X}_{M=1} - \mu_x}{s_{x_i}} \leq t\right) = 0.95 \tag{C-15}$$

and

$$Prob\left(-t \leq \frac{\bar{\bar{X}} - \mu_x}{s_{x_j}/\sqrt{M}} \leq t\right) = 0.95 \tag{C-16}$$

where the Student-*t* statistic is no longer equal to the standard *z*-score (1.96) as shown in Equation (C-13) because the variables $\frac{\bar{X}_{M=1}-\mu_x}{s_{x_i}}$ and $\frac{\bar{\bar{X}}-\mu_x}{s_{x_j}/\sqrt{M}}$ are not Gaussian distributed [C-1]. These variables instead follow the Student-*t* distribution with *N*-1 or *M*-1 degrees of freedom (ν), respectively. A table of values for the Student-*t* statistic can be found in Table A.2 of Appendix A of [C-1] or calculated directly using statistical functions for the inverse of the Student-*t* distribution.

The precision uncertainty for a sample mean from *N* finite measurements of *X* is assumed to follow a Student-*t* distribution, the precision uncertainty of the mean result is:

$$P_{\bar{x}} = ts_{\bar{x}} \tag{C-17}$$

where *t* is the coverage factor based on the degrees of freedom and confidence level (i.e. $t = t_{(\alpha/2,1=95\%,\nu)}$ for the inverse function for the Student-*t* distribution).

For *M*≥10, a coverage factor of 2 is advised. If *M*<10, a coverage factor of 2 is still acceptable if the bias and precision uncertainties are of similar magnitude. Coleman and Steele advise that the large sample equations (i.e. *t*=2) are applicable in the vast majority of engineering testing ([C-1], p. 85).

The precision uncertainties for each variable are then propagated through Equation (C-6), and the total uncertainty for the experimental result is:

$$U_r^2 = B_r^2 + P_r^2 \tag{C-18}$$

where $r \pm U_r$ provides a 95% confidence interval for the population mean, or true result. Alternate approaches used by ISO and ITTC combine the bias and precision uncertainties before expanding to 95% confidence intervals. This approach assumes the combined error distributions are Gaussian, even if the individual uncertainties are not. This approach also requires an estimate to approximate the effective degrees of freedom using the Welch-Satterthwaite formula.

The test results in this report are derived from multiple test runs performed using the same experimental apparatus and the final experimental results are given as the mean of the individual test run means. This allows the expanded precision uncertainty to be determined directly and independent of the bias uncertainty estimates. For a test results (*r*) that uses an equation involving a combination of measured test variables (*X*), a calculated result is determined from the mean measured test variables for each test run. With intermediate test results calculated for each test run, the precision uncertainty can be calculated directly for multiple test runs without the need to use the sensitivity coefficients for precision uncertainties as shown in Equations (C-

5) and (C-6). In an experiment where a test is run *M* times, resulting in individual mean values $\bar{r}_1, \bar{r}_2, \ldots, \bar{r}_M$ for the data reduction equation in Equation (C-1), the grand mean ($\bar{\bar{r}}$) of these multiple test runs produce a final "best" result as follows:

$$\bar{\bar{r}} = \frac{1}{M}\sum_{k=1}^{M} \bar{r}_k \qquad \text{(C-19)}$$

The bias uncertainty for this grand mean test result is the same as for a single test run, and determined using sensitivity coefficients described in C-3 and C-4. Bias uncertainties are fixed systematic errors, and are not affected by averaging the results of multiple test runs.

The standard deviation of the results from the *M* individual tests (with *M*-1 degrees of freedom) is given by:

$$S_r = \left[\frac{1}{M-1}\sum_{k=1}^{M} (\bar{r}_k - \bar{\bar{r}})^2\right]^{1/2} \qquad \text{(C-20)}$$

The standard deviation of the average result is then:

$$S_{\bar{r}} = \frac{S_r}{\sqrt{M}} \qquad \text{(C-21)}$$

And the overall precision uncertainty for the computed variable, *r* is:

$$P_{\bar{r}} = tS_{\bar{r}} \qquad \text{(C-22)}$$

The total uncertainty is then the same as Equation (C-18):

$$U_{\bar{r}}^2 = B_{\bar{r}}^2 + P_{\bar{r}}^2 \qquad \text{(C-23)}$$

In this method used for this experimental program, the overall precision uncertainty is computed directly, instead of being calculated for individual inputs and propagated through the data reduction equation (DRE) using sensitivity coefficients. This is method is also referred to as an "end-to-end" method. Coleman and Steele advise that when multiple samples of all the variables can be obtained over an appropriate time period, the direct determination method for P_r is advantageous due to the possibility that the random errors in different variables are correlated [C-1] (p. 105).

APPROACH

Total Resistance

The data reduction equation for total resistance (R_t) for the calm water *Athena* model data is:

$$R_t = F_{xfwd} + F_{xaft}\cos(\tau) + F_{zaft}\sin(\tau) \qquad \text{(C-24)}$$

where F_{xfwd} is the resistance measured at forward dynamometer, located under the tow post,

F_{xaft} is the resistance measured at aft dynamometer, located under the grasshopper; and

τ is the running trim angle.

The forward dynamometer is located above the model pivot point, so the direction is earth-fixed. The aft dynamometer is mounted to the model, so it needs to be corrected to earth-fixed resistance in the *x*-direction.

The total uncertainty for R_t is:

$$U_{R_t}^2 = B_{R_t}^2 + P_{R_t}^2 \tag{C-25}$$

The total bias uncertainty is:

$$B_{R_t}^2 = B_{F_{xfwd}}^2 \theta_{F_{xfwd}}^2 + B_{F_{xaft}}^2 \theta_{F_{xaft}}^2 + B_{F_{zaft}}^2 \theta_{F_{zaft}}^2 + B_\tau^2 \theta_\tau^2 \tag{C-26}$$

where the sensitivity coefficients for each variable are as follows:

$$\theta_{F_{xfwd}} = \frac{\partial R_T}{\partial F_{xfwd}} = 1 \tag{C-27}$$

$$\theta_{F_{xaft}} = \frac{\partial R_T}{\partial F_{xaft}} = \cos(\tau) \tag{C-28}$$

$$\theta_{F_{yaft}} = \frac{\partial R_T}{\partial F_{yaft}} = \sin(\tau) \tag{C-29}$$

$$\theta_\tau = \frac{\partial R_T}{\partial \tau} = -F_{xaft}\sin(\tau) + F_{zaft}\cos(\tau) \tag{C-30}$$

An additional error in the resistance measurement may result from a misalignment angle during installation (α). This misalignment error give a difference between the measured and actual force to as:

$$\Delta F = F_{xmeas} - F_{xmeas}\cos\alpha \tag{C-31}$$

with a misalignment bias uncertainty for each individual gage as follows:

$$B_\alpha^2 = B_{F_{xmeas}}^2 \theta_{F_{xmeas}}^2 + B_\alpha^2 \theta_\alpha^2 \tag{C-32}$$

where the sensitivity coefficients are:

$$\theta_{F_{xmeas}} = 1 - \cos\alpha \tag{C-33}$$

$$\theta_\alpha = -F_{xmeas}\sin\alpha \tag{C-34}$$

For small angles of 0.5 degrees or less (which is the inclinometer resolution), both Equations (C-33) and (C-34) approach zero and can be ignored in further uncertainty analysis.

Total Resistance Coefficient

The total uncertainty for C_T is:

$$U_{C_T}^2 = B_{C_T}^2 + P_{R_T}^2 \tag{C-35}$$

The total bias uncertainty is:

$$B_{C_T}^2 = B_S^2 \theta_S^2 + B_V^2 \theta_V^2 + B_{R_t}^2 \theta_{R_t}^2 + B_\rho^2 \theta_\rho^2 \tag{C-36}$$

where the sensitivity coefficients for each variable are as follows:

$$\theta_S = \frac{\partial C_T}{\partial S} = \frac{-R_t}{\frac{1}{2}\rho V^2 S^2} \tag{C-37}$$

$$\theta_V = \frac{\partial C_T}{\partial V} = \frac{-R_t}{\frac{1}{2}\rho V^3 S} \tag{C-38}$$

$$\theta_{R_t} = \frac{\partial C_T}{\partial R_x} = \frac{1}{\frac{1}{2}\rho V^2 S} \tag{C-39}$$

$$\theta_\rho = \frac{\partial C_T}{\partial \rho} = \frac{-R_t}{\frac{1}{2}\rho^2 V^2 S} \quad \text{(C-40)}$$

Friction Resistance Coefficient

The total uncertainty for C_F is:

$$U_{C_F}^2 = B_{C_F}^2 \quad \text{(C-41)}$$

The total bias uncertainty is:

$$B_{C_F}^2 = B_V^2\theta_V^2 + B_L^2\theta_L^2 + B_\nu^2\theta_\nu^2 \quad \text{(C-42)}$$

where the sensitivity coefficients for each variable are as follows:

$$\theta_V = \frac{\partial C_F}{\partial V} = 0.075\left(-\frac{2}{\left(Log\left(\frac{V * L_{pp}}{\nu}\right) - 2\right)^3}\right)\frac{1}{Vln(10)} \quad \text{(C-43)}$$

$$\theta_L = \frac{\partial C_F}{\partial L} = 0.075\left(-\frac{2}{\left(Log\left(\frac{V * L_{pp}}{\nu}\right) - 2\right)^3}\right)\frac{1}{L_{PP}ln(10)} \quad \text{(C-44)}$$

$$\theta_\nu = \frac{\partial C_F}{\partial \nu} = 0.075\left(-\frac{2}{\left(Log\left(\frac{V * L_{pp}}{\nu}\right) - 2\right)^3}\right)(-\frac{1}{\nu ln(10)}) \quad \text{(C-45)}$$

Residuary Resistance Coefficient

The total uncertainty for C_R is:

$$U_{C_R}^2 = B_{C_R}^2 \quad \text{(C-46)}$$

The total bias uncertainty is:

$$B_{C_R}^2 = B_{C_T}^2\theta_{C_T}^2 + B_{C_F}^2\theta_{C_F}^2 + B_S^2\theta_S^2 + B_{S_0}^2\theta_{S_0}^2 \quad \text{(C-47)}$$

where the sensitivity coefficients for each variable are as follows:

$$\theta_{C_T} = \frac{\partial C_R}{\partial C_T} = 1 \quad \text{(C-48)}$$

$$\theta_{C_F} = \frac{\partial C_R}{\partial C_F} = -\frac{S}{S_0} \quad \text{(C-49)}$$

$$\theta_S = \frac{\partial C_R}{\partial S} = -\frac{C_F}{S_0} \quad \text{(C-50)}$$

$$\theta_{S_0} = \frac{\partial C_R}{\partial S_0} = \frac{C_F * S}{S_0^2} \quad \text{(C-51)}$$

Bias uncertainty for *Fx* and *Fy* at the forward and aft position include the calibration errors for the dynamometers and the errors in the weights used for the calibration. The bias uncertainties are listed in Table C - 1. The second column in the table shows either the standard deviation of the instrument (s, from calibration, etc.) or the reported range (see "Notes" column for detail). If the standard deviation is given, the errors are assumed to be Gaussian and multiplied by 2 to yield the 95% confidence intervals. If the range is given, the errors are assumed to be uniform and divided by the square root of 3 [C-5] (Section 4.3.7).

Table C - 1. Uncertainties for Resistance Measurement

Description	S or Range	N	B*	Notes
Kistler 2003-3 *Fx* (fwd)	0.13 lbf	153	0.26	Calibration error, Gaussian
Kistler 2003-3 *Fy* (fwd)	0.08 lbf	153	0.16	Calibration error, Gaussian
Kistler 2003-4 *Fx* (aft)	0.11 lbf	152	0.22	Calibration error, Gaussian
Kistler 2003-4 *Fy* (aft)	0.14 lbf	152	0.28	Calibration error, Gaussian
Calibration weights	±0.10 lbf	n/a	0.06	Estimated by test engineer, rectangular
Wetted Surface Area	20 in^2	n/a	40	Estimated by test engineer, Gaussian
*B is estimated at 95% confidence interval				

Trim Angle from String Potentiometers

The data reduction equation for the running trim angle is as follows:

$$\tau = \operatorname{asin}\left(\frac{\sigma_{FSP} - \sigma_{ASP}}{L_{SP}}\right) \tag{C-52}$$

where σ_{FSP} sinkage at forward string potentiometer,

σ_{ASP} is the sinkage at aft string potentiometer, and

L_{FSP} is the distance between string potentiometers.

The total uncertainty for τ is:

$$U_{\bar{\tau}}^2 = B_{\tau}^2 + P_{\bar{\tau}}^2 \tag{C-53}$$

The total bias uncertainty is:

$$B_{\tau}^2 = B_{\sigma_{FSP}}^2 \theta_{\sigma_{FSP}}^2 + B_{\sigma_{ASP}}^2 \theta_{\sigma\ ASP}^2 + B_{L_{SP}}^2 \theta_{L_{SP}}^2 \tag{C-54}$$

where the sensitivity coefficients for each variable are as follows:

$$\theta_{\sigma_{FSP}} = \frac{\partial \tau}{\partial \sigma_{FSP}} = \frac{1}{L_{SP}\sqrt{1 - \left(\frac{\sigma_{FSP} - \sigma_{ASP}}{L_{SP}}\right)^2}} \tag{C-55}$$

$$\theta_{\sigma_{ASP}} = \frac{\partial \tau}{\partial \sigma_{ASP}} = \frac{1}{-L_{SP}\sqrt{1 - \left(\frac{\sigma_{FSP} - \sigma_{ASP}}{L_{SP}}\right)^2}} \tag{C-56}$$

$$\theta_{L_{SP}} = \frac{\partial \tau}{\partial L_{SP}} = \frac{\sigma_{FSP} - \sigma_{ASP}}{-L_{SP}^2\sqrt{1 - \left(\frac{\sigma_{FSP} - \sigma_{ASP}}{L_{SP}}\right)^2}} \tag{C-57}$$

Bias uncertainties for the running trim calculations include the string potentiometer calibration errors and the measurement error of the separation distance between the string potentiometers. These bias uncertainties are listed in Table C - 2.

Table C - 2. Uncertainties for Trim Measurement

Description	S or Range	N	B*	Notes
Fwd string pot	0.02 in	33	0.04 in	standard error of regression, Gaussian
Aft string pot	0.03 in	33	0.06 in	standard error of regression, Gaussian
Length between potentiometers	±1/16 in	n/a	0.04 in	estimated by test engineer, rectangular
*B is estimated at 95% confidence level				

Sinkage

The data reduction equation for the sinkage at LTP (σ_{LTP}) from the initial condition is:

$$\sigma_{LTP} = \sigma_{ASP} + X_{TP}\left(\frac{\sigma_{FSP} - \sigma_{ASP}}{L_{SP}}\right) \tag{C-58}$$

where σ_{FSP} is the sinkage at forward string potentiometer,

σ_{ASP} is the sinkage of aft string potentiometer,

L_{FSP} distance between string potentiometers, and

X_{TP} is the longitudinal position of tow point (measured along the model from aft potentiometer).

The total uncertainty for σ is:

$$U_{\bar{\sigma}}^2 = B_{\sigma}^2 + P_{\bar{\sigma}}^2 \tag{C-59}$$

The total bias uncertainty is:

$$B_{\sigma}^2 = B_{\sigma_{FSP}}^2\theta_{\sigma_{FSP}}^2 + B_{\sigma_{ASP}}^2\theta_{\sigma_{ASP}}^2 + B_{L_{SP}}^2\theta_{L_{SP}}^2 \tag{C-60}$$

where the sensitivity coefficients for each variable are as follows:

$$\theta_{\sigma_{FSP}} = \frac{\partial\sigma_{TP}}{\partial\sigma_{FSP}} = \frac{X_{TP}}{L_{SP}} \tag{C-61}$$

$$\theta_{\sigma_{ASP}} = \frac{\partial\sigma_{TP}}{\partial\sigma_{ASP}} = 1 - \frac{X_{TP}}{L_{SP}} \tag{C-62}$$

$$\theta_{L_{SP}} = \frac{\partial\sigma_{TP}}{\partial L_{SP}} = -\frac{X_{TP}(\sigma_{FSP} - \sigma_{ASP})}{L_{SP}^2} \tag{C-63}$$

Bias uncertainties for the sinkage calculation include the string potentiometer calibration errors, the measurement error of the separation distance between the string potentiometers, and the uncertainty in the LTP measurement. These bias errors are listed in Table C - 3.

Table C - 3. Uncertainties for Sinkage Measurement

Description	S or Range	N	B*	Notes
Fwd string pot	0.02 in	33	0.040 in	Standard error of regression, Gaussian
Aft string pot	0.03 in	33	0.060 in	Standard error of regression, Gaussian
Length between potentiometers	±1/16 in	n/a	0.040 in	Estimated by test engineer, rectangular
LCG	n/a	n/a	0.10 in	See description below
*B is estimated at 95% confidence level				

Mass Properties

Table C - 4 shows the uncertainties used to calculate model mass properties.

Table C - 4. Uncertainties for Instrumentation in Calculation of Model Mass Properties

Description	S or Range	B	Notes
Individual trim and ballast weights	0.10 lb	0.058 lb	Estimated by test engineer, uniform rectangular distribution
Individual tape measure measurements	0.063 in	0.036 in	Estimated by test engineer, uniform rectangular distribution
Individual weight measurements of model components	0.50 lb	0.30 lb	Transducer Techniques MLP-500 load cell calibration, uniform rectangular distribution
Relative trim angle for inclining measurements	0.50º	0.30º	Wyler inclinometer specifications, Gaussian
relative trim angle for VCG	n/a	0.058º	Estimated by test engineer, uniform rectangular distribution
*B is estimated at 95% confidence level			

Weight

The weight of the model is determined by the summation of the weights, as shown Equation (C-47):

$$W_M = \sum_{i=1}^{n} W_i \tag{C-64}$$

where W_M is the total weight of the model, and W_i are the individual components.

The bias uncertainty for model weight becomes the sum of the individual weight bias uncertainties because the partial derivatives of Equation (C-47) with respect to the individual weights are all 1:

$$B_M^2 = \sum_{i=1}^{n} B_i^2 \tag{C-65}$$

Table C - 5 shows the bias uncertainties for the individual components of the bias uncertainty for weight, as well as the resultant overall model uncertainty. The uncertainty the model weight is the dominating factor.

Table C - 5. Uncertainty in As-Tested Weight Items

Description	S or Range (lb)	B* (lb)
Model hull, ballast, and instrumentation as-rigged	0.50	0.29
Removed trimming weights	0.10	0.058
Heave post as-rigged	0.10	0.058
Overall	n/a	0.31
*B is estimated at 95% confidence level		

Center of Gravity (CG)

The center of gravity (CG) of the model is determined by suspending the model and a beam beneath an A-frame, attached to a swing pivot. The model is leveled by adding trim weights with the trim angle measured with an inclinometer. Once the model is level, the longitudinal center of gravity (LCG) is then located under the swing pivot point. The trim weights are then removed computationally to determine the final CG. CG uncertainty analysis is conducted via linear regression using the following data reduction equation per Coleman and Steele [C-1]:

$$\begin{aligned}(Y_i) = (m) * (X_i) + (c) \xrightarrow{variable\ sub.} \underbrace{\left(\frac{w_i * d_i}{W_{tot}}\right)}_{Y_i} \\ = \underbrace{(VCG)}_{m} * \underbrace{(\tan \alpha_i)}_{X_i} + \underbrace{(LCG)}_{c}\end{aligned} \tag{C-66}$$

where VCG is the vertical center of gravity of the hull, beam and inclining weight,

LCG is the longitudinal center of gravity of the hull, beam and inclining weight,

w_i is the weight of the *i*th trim weight,

d_i is the distance from CG of the *i*th trim weight,

α_i is the angle caused by placing the trim weight (w) a distance (d) from the CG, and

W_{tot} is the total weight including the hull, the beam, and the inclining weight.

Figure C - 1 shows an inclining plot of $\left(\frac{w_i * d_i}{W_{tot}}\right)$ $\boldsymbol{vs.}$ $(\tan \alpha_i)$. Each of the points represents one of the trim weight movements. The slope of the linear regression line is the *VCG* and the Y-axis intercept is the *LCG*. This method is common naval architecture practice and considered statistically robust as it includes the regression error when calculating *VCG*.

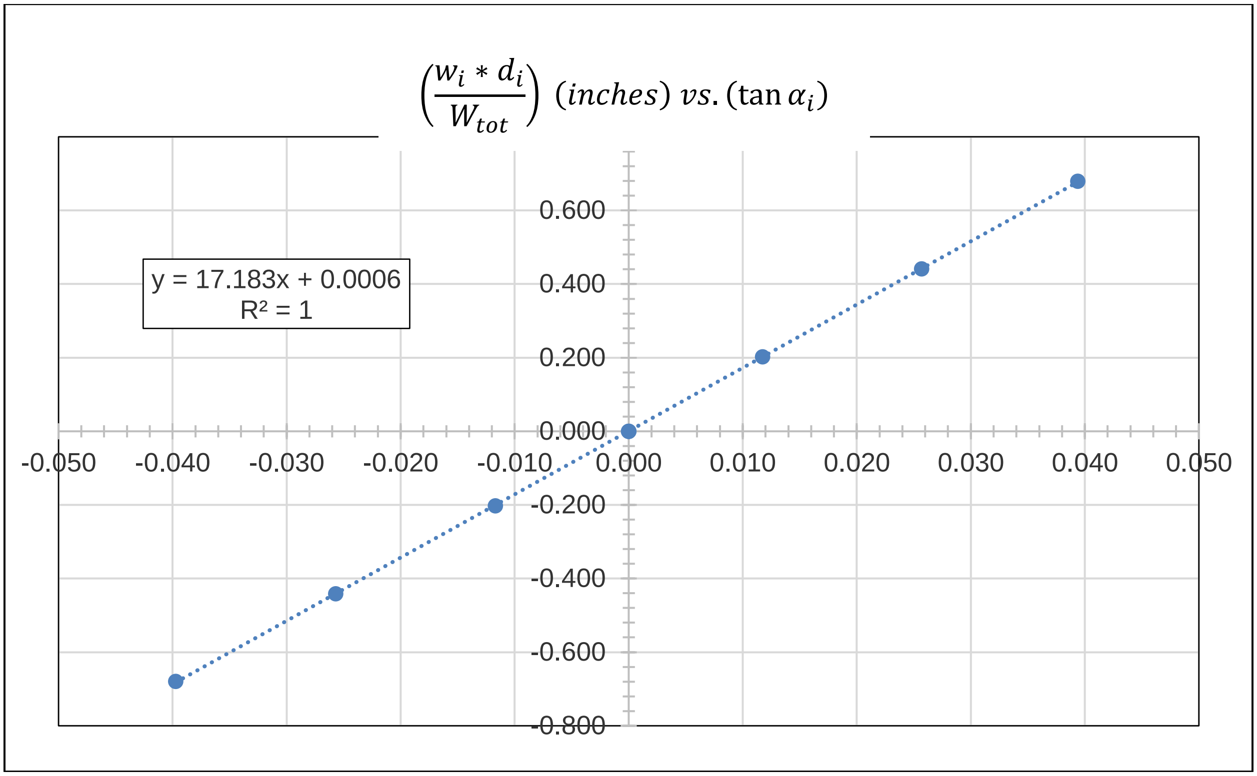

Figure C - 1. Inclining Plot of (w_i*d_i/W_{tot}) vs (tan α_i)

Vertical Center of Gravity (VCG)

Solving for linear regression slope in the inclining plot gives data reduction equation (DRE) for the vertical center of gravity (VCG) as follows:

$$m = \frac{(Y_i - c)}{X_i} = \frac{\Delta Y}{\Delta X} \xrightarrow{variable\ sub.} \underbrace{VCG}_{m} = \frac{\overbrace{\left\{\left(\frac{w * d}{W_{tot}}\right)_{max} - \left(\frac{w * d}{W_{tot}}\right)_{min}\right\}}^{\Delta Y}}{\underbrace{\{\tan \alpha_{max} - \tan \alpha_{min}\}}_{\Delta X}} \quad \text{(C-67)}$$

Partial derivatives of the DRE give sensitivity coefficients (θ_j) for the regression slope as shown in [C-1] section 7-4.1. The regression slope is dependent upon the spread of data rather than on a point value (or mean value) within the data set. Therefore, the partial derivatives are performed with respect to ΔX and ΔY, and the sensitivity coefficients are evaluated at the minimum and maximum values of d and α. Assuming ΔX and ΔY are uncorrelated, the partial derivatives of regression slope are as follows:

$$\theta_Y = \frac{\partial m}{\partial \Delta Y} = \frac{\partial (VCG)}{\partial \left(\left\{\left(\frac{w * d}{W_{tot}}\right)_{max} - \left(\frac{w * d}{W_{tot}}\right)_{min}\right\}\right)} = \frac{1}{\{\tan \alpha_{max} - \tan \alpha_{min}\}} \quad \text{(C-68)}$$

$$\theta_X = \frac{\partial m}{\partial \Delta X} = \frac{\partial (VCG)}{\partial (\{\tan \alpha_{max} - \tan \alpha_{min}\})} = -\frac{\left\{\left(\frac{w * d}{W_{tot}}\right)_{max} - \left(\frac{w * d}{W_{tot}}\right)_{min}\right\}}{(\{\tan \alpha_{max} - \tan \alpha_{min}\})^2} \quad \text{(C-69)}$$

The precision (random) and bias (systematic) uncertainties of the regression slope are derived as follows from equation (7.27) in reference [C-1]:

$$P_{VCG}{}^2 = t^2(s_Y^2\theta_Y^2 + s_X^2\theta_X^2) \tag{C-70}$$

$$B_{VCG}{}^2 = B_Y^2\theta_Y^2 + B_X^2\theta_X^2 \tag{C-71}$$

where the linear regression standard error for *y* is

$$s_Y^2 = \frac{1}{N-2}\sum_{i=1}^{N}(Y_i - \hat{Y}_i)^2$$

And the linear regression standard error for *x* is

$$s_X^2 = \frac{1}{N-2}\sum_{i=1}^{N}(X_i - \hat{X}_i)^2$$

The total uncertainty for *VCG* (below the swing pivot point) is:

$$U_{VCG}^2 = B_{VCG}^2 + P_{VCG}^2 \tag{C-72}$$

Table C - 6. Uncertainty for *VCG*: As-Inclined

Description	Value
$B_Y^2\theta_Y^2$	0.00074 in^2
$B_X^2\theta_X^2$	0.048 in^2
B_{VCG}	±0.22 in
P_{VCG}	±0.067 in
U_{VCG}	±0.23 in

VCG uncertainty of the hull and beam without the inclining weights is determined via the following data reduction equation:

$$VCG1 = \frac{W_{tot}\,VCG - w\,z_w}{W_m} \tag{C-73}$$

where *VCG1* is the hull and beam vertical center of gravity below the swing pivot point,

z_w is the inclining weight vertical center of gravity below the swing pivot point, and

W_m is the weight of the hull and beam.

Partial derivatives of the DRE give sensitivity coefficients (θ_j) as follows:

$$\theta_{W_{tot}} = \frac{\partial VCG1}{\partial W_{tot}} = \frac{VCG}{W_m} \tag{C-74}$$

$$\theta_{VCG} = \frac{\partial VCG1}{\partial VCG} = \frac{W_{tot}}{W_m} \tag{C-75}$$

$$\theta_w = \frac{\partial VCG1}{\partial w} = -\frac{z_w}{W_m} \tag{C-76}$$

$$\theta_{z_w} = \frac{\partial VCG1}{\partial z_w} = -\frac{w}{W_m} \qquad \text{(C-77)}$$

$$\theta_{W_m} = \frac{\partial VCG1}{\partial W_m} = -\frac{W_{tot}\, VCG - w\, z_w}{{W_m}^2} \qquad \text{(C-78)}$$

Table C - 7. Uncertainty for *VCG1*: As-Inclined Without Inclining Weights

Description	Value
$B^2_{W_{tot}}\theta^2_{W_{tot}}$	1.19E-05 in^2
$B^2_{VCG}\theta^2_{VCG}$	5.44E-02 in^2
$B^2_{w}\theta^2_{w}$	5.73E-08 in^2
$B^2_{z_w}\theta^2_{z_w}$	1.14E-06 in^2
$B^2_{W_m}\theta^2_{W_m}$	1.12E-05 in^2
B_{VCG1}	±0.23 in
P_{VCG1}	±0.0 in
U_{VCG1}	±0.23 in

VCG uncertainty of the hull without the inclining weights, beam, or tow post are determined via the following data reduction equation:

$$VCG'o = \frac{W_m\, VCG1 - W_b\, VCG_b}{W_{hull}} \qquad \text{(C-79)}$$

where VCG'_o is the hull vertical center of gravity below the swing pivot point,

VCG_b is the beam vertical center of gravity below the swing pivot point,

W_b is the weight of the beam, and

W_{hull} is the weight of the hull.

Partial derivatives of the DRE give sensitivity coefficients (θ_j) as follows:

$$\theta_{W_m} = \frac{\partial VCG'o}{\partial W_m} = \frac{VCG1}{W_{hull}} \qquad \text{(C-80)}$$

$$\theta_{VCG1} = \frac{\partial VCG'o}{\partial VCG1} = \frac{W_m}{W_{hull}} \qquad \text{(C-81)}$$

$$\theta_{W_b} = \frac{\partial VCG'o}{\partial W_b} = -\frac{VCG_b}{W_{hull}} \qquad \text{(C-82)}$$

$$\theta_{VCG_b} = \frac{\partial VCG'o}{\partial VCG_b} = -\frac{W_b}{W_{hull}} \qquad \text{(C-83)}$$

$$\theta_{W_{hull}} = \frac{\partial VCG'o}{\partial W_{hull}} = -\frac{W_m\, VCG1 - W_b VCG_b}{{W_{hull}}^2} \qquad \text{(C-84)}$$

Table C - 8. Uncertainty for *VCG'$_o$*: As-Inclined Without Inclining Weights and Support Beam

Description	Value
$B^2_{W_m}\theta^2_{W_m}$	1.74E-05 in^2
$B^2_{VCG1}\theta^2_{VCG1}$	8.46E-02 in^2
$B^2_{w_b}\theta^2_{w_b}$	1.14E-06 in^2
$B^2_{VCG_b}\theta^2_{VCG_b}$	7.32E-04 in^2
$B^2_{W_{hull}}\theta^2_{W_{hull}}$	4.87E-05 in^2
$B_{VCG'o}$	±0.29 in
$P_{VCG'o}$	±0.0 in
$U_{VCG'o}$	±0.29 in

VCG uncertainty of the hull above the baseline is determined via the following data reduction equation:

$$VCGo\ = z_{LB} - VCG'o \tag{C-85}$$

where VCG_o is the hull vertical center of gravity above the baseline, and

z_{BL} is the height of the swing pivot point above the baseline.

Partial derivatives of the DRE give sensitivity coefficients (θ_j) as follows:

$$\theta_{z_{BL}} = \frac{\partial VCGo}{\partial z_{BL}} = 1 \tag{C-86}$$

$$\theta_{VCG'o} = \frac{\partial VCGo}{\partial VCG'o} = -1 \tag{C-87}$$

Table C - 9. Uncertainty for *VCG$_o$*: As-Inclined Without Inclining Weights and Support Beam above Baseline

Description	Value
$B^2_{VCG'o}\theta^2_{VCG'o}$	0.085 in^2
$B^2_{z_{BL}}\theta^2_{z_{BL}}$	0.063 in^2
B_{VCGo}	±0.39 in
P_{VCGo}	±0.0 in
U_{VCGo}	±0.39 in

VCG uncertainty for the additional weight items not onboard the model during the inclining experiment must also be included in the as-tested uncertainty. This is represented using the following data reduction equation:

$$VCG_M = \sum_{i=1}^{n} VCG_i \frac{W_i}{W_M} \tag{C-88}$$

where VCG_i is the vertical center of gravity of the individual weights above the baseline.

The total bias uncertainty due to the total model weight (M), the tow post weight (TP) and the dry hull weight (hull) is then given as follows:

$$B_{VCG_M}^2 = B_{W_i}^2\theta_{W_i}^2 + B_{z_i}^2\theta_{z_i}^2 + B_{W_M}^2\theta_{W_M}^2 \quad \text{(C-89)}$$

where the sensitivity coefficients are:

$$\theta_{W_i} = \frac{VCG_{TP}}{W_M} + \frac{VCGo}{W_M} \quad \text{(C-90)}$$

$$\theta_{z_i} = \frac{W_{TP}}{W_M} + \frac{W_{hull}}{W_M} \quad \text{(C-91)}$$

$$\theta_{W_M} = -\frac{VCG_{TP}W_{TP}}{W_M^2} + -\frac{VCGoW_{hull}}{W_M^2} \quad \text{(C-92)}$$

Table C - 10. Uncertainty for *VCG*: As-Tested above Baseline

Description	Value
$B_{W_i}^2\theta_{W_i}^2$	1.14E-05 in^2
$B_{z_i}^2\theta_{z_i}^2$	1.42E-01 in^2
$B_{W_M}^2\theta_{W_M}^2$	1.11E-05 in^2
B_{VCG_M}	±0.38 in

Longitudinal Center of Gravity (LCG)

LCG uncertainty of the hull and beam without the inclining weights is determined via the following data reduction equation:

$$LCG1 = \frac{W_{tot}LCG - w\,y_w}{W_m} \quad \text{(C-93)}$$

where *LCG1* is the hull and beam longitudinal center of gravity forward of the swing pivot point, and

y_w is the inclining weight longitudinal center of gravity forward of the swing pivot point.

Partial derivatives of the DRE give sensitivity coefficients (θ_j) as follows:

$$\theta_{W_{tot}} = \frac{\partial LCG1}{\partial W_{tot}} = \frac{LCG}{W_m} \quad \text{(C-94)}$$

$$\theta_{LCG} = \frac{\partial LCG1}{\partial LCG} = \frac{W_{tot}}{W_m} \quad \text{(C-95)}$$

$$\theta_w = \frac{\partial LCG1}{\partial w} = -\frac{y_w}{W_m} \quad \text{(C-96)}$$

$$\theta_{y_w} = \frac{\partial LCG1}{\partial y_w} = -\frac{w}{W_m} \quad \text{(C-97)}$$

$$\theta_{W_m} = \frac{\partial LCG1}{\partial W_m} = -\frac{W_{tot}\,LCG - w\,y_w}{{W_m}^2} \quad \text{(C-98)}$$

Table C - 11. Uncertainty for *LCG1*: As-Inclined Without Inclining Weights

Description	Value
$B^2_{W_{tot}}\theta^2_{W_{tot}}$	1.30E-14 in^2
$B^2_{LCG}\theta^2_{LCG}$	3.41E-04 in^2
$B^2_{w}\theta^2_{w}$	0.0 in^2
$B^2_{y_w}\theta^2_{y_w}$	5.69E-07 in^2
$B^2_{W_m}\theta^2_{W_m}$	1.23E-14 in^2
B_{LCG1}	±0.019 in
P_{LCG1}	±0.0 in
U_{LCG1}	±0.019 in

LCG uncertainty of the hull without the inclining weights, beam, or tow post are determined via the following data reduction equation:

$$LCG'o = \frac{W_m\ LCG1 - W_b\ LCG_b}{W_{hull}} \tag{C-99}$$

where *LCG'o* is the hull longitudinal center of gravity forward of the swing pivot point, and

LCG_b is the beam longitudinal center of gravity forward of the swing pivot point.

Partial derivatives of the DRE give sensitivity coefficients (θ_j) as follows:

$$\theta_{W_m} = \frac{\partial LCG'o}{\partial W_m} = \frac{LCG1}{W_{hull}} \tag{C-100}$$

$$\theta_{LCG1} = \frac{\partial LCG'o}{\partial LCG1} = \frac{W_m}{W_{hull}} \tag{C-101}$$

$$\theta_{W_b} = \frac{\partial LCG'o}{\partial W_b} = -\frac{LCG_b}{W_{hull}} \tag{C-102}$$

$$\theta_{LCG_b} = \frac{\partial LCG'o}{\partial LCG_b} = -\frac{W_b}{W_{hull}} \tag{C-103}$$

$$\theta_{W_{hull}} = \frac{\partial LCG'o}{\partial W_{hull}} = -\frac{W_m\ LCG1 - W_b LCG_b}{{W_{hull}}^2} \tag{C-104}$$

Table C - 12. Uncertainty for *LCG'o*: As-Inclined Without Inclining Weight and Support Beam

Description	Value
$B^2_{W_m}\theta^2_{W_m}$	1.91E-14 in^2
$B^2_{LCG1}\theta^2_{LCG1}$	5.30E-04 in^2
$B^2_{w_b}\theta^2_{w_b}$	6.52E-14 in^2
$B^2_{LCG_b}\theta^2_{LCG_b}$	9.17E-06 in^2
$B^2_{W_{hull}}\theta^2_{W_{hull}}$	2.39E-14 in^2
$B_{LCG'o}$	±0.023 in
$P_{LCG'o}$	±0.0 in
$U_{LCG'o}$	±0.023 in

LCG uncertainty of the hull relative to the baseline is determined via the following data reduction equation:

$$LCGo\ = x_{TKI} - LCG'o \tag{C-105}$$

where *LCGo* is the longitudinal center of gravity forward of the aft perpendicular, and

x_{AP} is the horizontal distance of the swing pivot point forward of the aft perpendicular.

Partial derivatives of the DRE give sensitivity coefficients (θ_j) as follows:

$$C_{x_{TKI}} = \frac{\partial LCGo}{\partial x_{TKI}} = 1 \tag{C-106}$$

$$C_{\ LCG'o} = \frac{\partial LCGo}{\partial LCG'o} = -1 \tag{C-107}$$

Table C - 13. Uncertainty for LCG_o: As-Inclined Without Inclining Weight and Support Beam Forward of Aft Perpendicular

Description	Value
$B^2_{LCG'o}\theta^2_{LCG'o}$	0.023 in^2
$B^2_{x_{TKI}}\theta^2_{x_{TKI}}$	0.0039 in^2
B_{LCGo}	±0.067 in
P_{LCGo}	±0 in
U_{LCGo}	±0.067 in

The *LCG* uncertainty of the additional weight items not onboard the model during the inclining experiment must also be included in the as-tested uncertainty. The equation for corresponding data reduction equation is similar to the *VCG* calculation, where *z* was replaced by *x*:

$$LCG_M\ = \sum_{i=1}^{n} LCG_i \frac{W_i}{W_M} \tag{C-108}$$

where LCG_i is the longitudinal center of gravity of the individual weights forward of the aft perpendicular. The total bias uncertainty due to the model weight (M), the tow post weight (TP), and the dry hull weight (H) are given as follows:

$$B^2_{LCG_M} = B^2_{W_i}\theta^2_{W_i} + B^2_{x_i}\theta^2_{x_i} + B^2_{W_M}\theta^2_{W_M} \tag{C-109}$$

where the sensitivity coefficients were:

$$\theta_{W_i} = \frac{LCG_{TP}}{W_M} + \frac{LCGo}{W_M} \tag{C-110}$$

$$\theta_{x_i} = \frac{W_{TP}}{W_M} + \frac{W_{hull}}{W_M} \tag{C-111}$$

$$\theta_{W_m} = \frac{-LCG_{TP}W_{TP}}{W_M^2} + \frac{-LCGoW_{hull}}{W_M^2} \tag{C-112}$$

Table C - 14. Uncertainty for *LCG*: As-Tested Forward of Aft Perpendicular

Description	Value
$B_{W_i}^2 \theta_{W_i}^2$	1.26E-03 in^2
$B_{x_i}^2 \theta_{x_i}^2$	4.27E-03 in^2
$B_{W_M}^2 \theta_{W_M}^2$	1.15E-03 in^2
B_{LCG_M}	±0.082 in

Carriage Speed

The uncertainty in the carriage speed is comprised of the precision uncertainty for each run, along with the bias uncertainty derived from the encoder calibration. Table C - 15 shows the bias uncertainty from this carriage wheel encoder calibration.

Table C - 15. Uncertainties for Carriage Speed

Description	S or Range (kts)	N	B*	Notes
Calibration of encoder	1.58E-4	10	3.15E-4	Standard error of regression, Gaussian
*B is estimated at 95% confidence interval				

REFERENCES

[C-1] Coleman, H. and W. G. Steele, *Experimentation and Uncertainty Analysis for Engineers*, Second Edition, John Wiley and Sons, New York, 1999.

[C-2] American National Standards Institute/American Society of Mechanical Engineers. *Test Uncertainty*, PTC 19.1-1998, ASME, New York, 1998.

[C-3] American National Standards Institute/American Society of Mechanical Engineers. *Test Uncertainty*, PTC 19.1-1985 Part 1, ASME, New York, 1986.

[C-4] American Institute of Aeronautics and Astronautics, Assessment of Wind Tunnel Data Uncertainty, AIAA Standard S-071-1995, AIAA, New York, 1995.

[C-5] International Organization for Standardization, *Guide to the Expression of Uncertainty in Measurement*, ISBN 92-67-10188-9, ISO, Geneva, 1993, corrected and reprinted, 1995.

THIS PAGE INTENTIONALLY LEFT BLANK

Distribution

SPONSOR	Hard Copies #	Digital Copies #	NSWC, CARDEROCK DIVISION INTERNAL DISTRIBUTION Code	Name	Hard Copies	Digital Copies #
Office of Naval Research Division 333			809	D. Intolubbe	1	1
Attn: Dr. Robert Brizzolara		1	83	Technical Data Repository		1
Attn: Dr. Thomas Fu		1	8311	A. Jacobson		1
875 North Randolph Street Suite 1425			8314	C. Schleicher		1
Arlington, VA, 22203			8321	E. Lee		1
Defense Technical Information Center (DTIC)		1	808	J. Geiser		1
8725 John Kingman Road			863	D. Walker		1
Fort Belvoir, VA 22000-6218			863	S. Punzi		1
University of Iowa		1	881	C. Weil		1
Attn: Dr. Frederick Stern			881	J. Morin		1
			744	A. Fullerton		1
			Retired	C. Merrill		1
			1033	TIC-SCRIBE		1

THIS PAGE INTENTIONALLY LEFT BLANK

NAVSEA
WARFARE CENTERS
Carderock